(1)

Mississippi State University

Center for Air Sea Technology

OBJECTIVE FEATURE IDENTIFICATION AND TRACKING: A REVIEW

by
Ranjit M. Passi and Harsh Anand

Technical Report 94-4

15 September 1994

TECHNICAL REPORT 04-94

OBJECTIVE FEATURE IDENTIFICATION AND TRACKING: A REVIEW

by

Ranjit M. Passi[1] and Harsh Anand[2]

[1]University of Southern Mississippi Center for Ocean & Atmospheric Modeling, Stennis Space Center, MS 39529

[2]Mississippi State University Center for Air Sea Technology, Stennis Space Center, MS 39529

15 September 1994

This research was supported by the Department of the Navy, Office of the Chief of Naval Research under Research Grants N00014-92-J-4112 with the University of Southern Mississippi, and N00014-92-J-4109 with Mississippi State University. The opinion, findings, conclusions, and recommendations expressed in this publication are those of the authors and do not necessarily reflect the views of the U.S. Government. No official endorsement should be inferred.

ABSTRACT

Remote sensing of the oceans via satellites is providing useful data that can be used for realtime input into and verification of the numerical ocean models. To make an optimum use of these data, efficient methods are being developed to handle vast amounts of data and provide their quick analyses and summaries in the form of mesoscale features.

Identification, isolation and tracking of mesoscale features plays an important role in numerical ocean modeling. Of late, there has been considerable interest in designing algorithms to automatically detect such oceanographic features as temperature fronts and eddies. This report provides a literature review of recent approaches and efforts on objective feature identification (OFI) as it pertains to oceanographic applications. Most of the OFI work in oceanography has been done on characterizing the Gulf Stream (GS); and since the GS incorporates all the mesoscale feature complexities that one may desire to resolve, the literature reviewed here pertains to this feature entirely. It is felt that the work cited is quite representative and is applicable to other geographical features of interest.

Feature identification from satellite data can be viewed as a four-step process: (1) edge detection – analyzes pixels in satellite images for frontal boundaries; (2) edge labeling – assigns feature labels to frontal pixels; (3) spatial interpolation – fills spatial gaps in labeled features due to clouds or data sparsity; and (4) expert system – provides additional interpolation over space and time based on knowledge of the region dynamics. Most research efforts are focused on algorithm development for individual steps. Considerable effort is required to put together a complete system that can go from raw, satellite imagery to a finished product in terms of digitized information on frontal location and dynamics. The Navy's Semi-Automated Mesoscale Analysis System (SAMAS) is perhaps the only system that has combined these steps in a modular approach. The only other image analysis system is that of the University of Rhode Island (URI), which emphasizes the removal of clouds from AVHRR images to enhance edge detection.

This review describes how different algorithms and approaches are being used in objective feature identification. After reviewing algorithms for the four steps individually, brief descriptions of SAMAS and the URI image analysis system are provided. Finally, methods of feature extraction and eddy tracking from model output are described. The Center for Air Sea Technology (CAST) has implemented these algorithms for oceanographic visualization.

TABLE OF CONTENTS

1. INTRODUCTION

Because of the ever-increasing amount of satellite-derived data available and because computers have become faster and less expensive, there is a rising interest in designing algorithms to automatically detect oceanographic features such as temperature fronts and eddies. This paper provides a literature review of recent approaches and efforts on objective feature identification (OFI) pertaining to oceanographic applications.

Characterization of ocean front and eddy features plays an important role in numerical ocean modeling. For instance, the objectively-determined location and size of an eddy can be directly assimilated into a numerical ocean model using a 'feature' model (Robinson and Walstad, 1987). The location of the North Wall (NW) of the Gulf Stream (GS) is used to separate water masses for input to the Optimum Thermal Interpolation System (OTIS) analyses of the GS region (Cummings, 1991). Such OTIS analyses, using the GS North Wall (GSNW) location, were used for model initialization in DAMEE-GSR (Data Assimilation and Model Evaluation Experiments – Gulf Stream Region); see Perkins (1993) for details.

Objectively-determined ocean features also play an important role in the objective evaluation of numerical ocean models. Often, the performance of a numerical model is defined in terms of its capability to reproduce certain observed, quantifiable features. Model output is analyzed to quantify the characteristic feature and compared with the objectively-derived feature from observations. In DAMEE-GSR, the GSNW location has been used for an assessment of ocean models prediction performance (Perkins, 1993; Fox et al., 1991).

For feature extraction from satellite observations or three-dimensional model output, computer based algorithms can be used to exploit the physical characteristics of the observations. The development of such algorithms requires that a feature be specified formally in terms of its defining characteristics. Given a set of sample values of a scalar field $f(x, y, z)$ over a volume, a feature is defined to be a region in the volume that has similar characteristics (Moorhead and Zhu, 1993). Formally, if the volume $\mathcal{V}$ is constituted by functional values of f that are bounded, then a feature may be defined as follows:

- a temporally-dynamic region $\mathcal{R} \in \mathcal{V}$ with all sample values belonging to a specified range $\mathcal{G}$, or
- a region $\mathcal{R} \in \mathcal{V}$ with sample values significantly different from the neighboring regions.

In the first case, features are defined in terms of the original sample values; the computer extracts the subset $\mathcal{R}$ easily in terms of the defining characteristic specified by $\mathcal{G}$. A well-known example of such a feature is the subsurface GSNW defined as the 15 deg isotherm at 200 m depth. This subset is easily extracted from a three-dimensional gridded model output. In the second case, features are not defined by the original sample values but by the region edges. This property characterizes features as only those regions that exhibit significant differences from the surrounding values; or equivalently, these regions can be identified because of the sharp edges (boundaries).

According to Lybanon and Holyer (1991), generation of oceanographic products from the interpretation of satellite data is a three-level image resolution paradigm: (1) edge detection, (2) edge labeling, and (3) feature construction. The edge detection level is the lowest, which works at the pixel level to derive feature edges or boundaries. These edges are disjoint. To join or fill in these disjoint edges, the next step is to label them corresponding to the features they represent. The final step is to fill in the gaps using spatial interpolation. In addition to these three levels, Lybanon and Holyer (1991) include a fourth level, viz., the expert system, which provides temporal interpolation during time periods of sparse observations. The expert system's rule base represents oceanographic knowledge about the evolution of mesoscale ocean features in terms of their kinematics. These four steps form the Four-Tiered Approach for the development of the Navy's Semi-Automated Mesoscale Analysis System (SAMAS) (Peckinpaugh and Holyer, 1991).

Considerable work has been done in each of the above categories separately; however, there has been a notable lack of effort in putting an overall system together that is capable of systematically converting raw images of satellite data into a finished picture which delineates all major features. In oceanographic applications, there are two different systems that are in the forefront. One is the Navy's SAMAS (Holyer and Peckinpaugh, 1990; Krishnakumar et al., 1990a) in which most of the components are well identified and tested. The expert system component still needs to be developed. The other system is being developed at University of Rhode Island (URI). URI has performed considerable analyses of the satellite AVHRR images, but it has been limited to providing labeled edges of the features.

In the edge labeling component, SAMAS uses the Relaxation Labeling Algorithm, which is an iterative procedure based on Bayes' Theorem (Krishnakumar et al., 1990a). Correspondingly, URI has the Contour-Following Algorithm, which restricts the rate of change with which the contour-curvature can vary spatially. For spatial interpolation, SAMAS employs an algorithm developed by Molinelli and Flanigan (1987) which is based on complex empirical orthogonal functions. Evidently, there are some gaps beyond this stage that need to be filled. The review will be cast in terms of the components of the two systems. It will include some algorithms which could possibly indicate direction for the development of the expert systems using the space-time interpolation concept.

The intent of this publication is to show how different approaches and modules can be put together for the OFI process by reviewing a few typical algorithms from each category. The discussion brings out the essence of each approach by including all relevant details of the illustrating algorithm chosen. This will provide the reader with a full flavor of the capabilities as well as the intricacies of the procedures. However, the review, by design, is not comprehensive.

Most of the techniques appearing in the literature on objective identification of ocean features are based on satellite observations of sea-surface temperature (SST) and sea-surface height (SSH) information from GEOSAT and pertain to the Gulf Stream region. Section 2 gives a description of the two types of satellite data, followed in Section 3 by a few conventional definitions of the terms used. Section 4 then describes the edge detection approaches including the Cluster Shade Algorithm due to Holyer and Peckinpaugh (1989) and the URI algorithm which is based on objective statistical tests for sequential decision making (Cornillon and Watts, 1987; Cayula and Cornillon, 1992). Section 5 covers the feature labeling approach and basically includes the Relaxation Labeling Algorithm adopted by the Navy (Krishnakumar et al., 1990a). The spatial interpolation algorithms are described in Section 6. The section reviews the complex empirical orthogonal functions (CEOF) approach of Molinelli and Flanigan (1987), the Pathfinder algorithm (Horton, 1989) and, more importantly, includes the description of work on space-time interpolation (Mariano, 1990; Chin and Mariano 1993).

With this development at hand, we give in Section 7, a brief description of the Navy and the URI systems in their modular form. As a complete system, it is pertinent to include the approach of dynamic interpolation where a numerical model, capable of reproducing the feature of the region, ingests observations (data assimilation) and predicts the required location of the feature. Finally, in Section 8 we describe an effort of feature extraction from 4-D model outputs available on a regular grid. The Center for Air Sea Technology has implemented these techniques in a visualization case study using the DieCAST model for the Gulf of Mexico (Dietrich et al., 1993). The three-dimensional features of the eddies extracted are sharp, and these eddies are tracked well as they traverse toward the western Gulf.

2. SATELLITE OBSERVATIONS

Apart from satellite data, observations of the ocean are quite sparse and inadequate to com-

pletely determine mesoscale ocean features. Therefore, investigators must depend on satellite observations that are abundantly available. For their optimal utilization in feature identification and nowcast/forecast activity, their inherent characteristics, advantages and drawbacks must be understood fully.

Altimetry from satellites, like GEOSAT, provides global coverage. However, these data are available only along satellite tracks that are separated by distances comparable to the dominant scales in the GS regime. Another problem associated with the use of altimetry is that the relationship of the measured SSH to the geoid is unknown. Subtraction of the time-averaged altimetry data from the satellite track data removes the geoid, but the mean ocean circulation signal is removed as well. In spite of these limitations, satellite SSH data have proved useful in data assimilation studies and in the determination of sea surface variability.

Multichannel SSTs from satellite IR images provide global coverage of the World Ocean. The images can be used subjectively or objectively to locate the position of the GSNW. However, SST data may be incomplete due to cloud cover, and atmospheric moisture contamination may not be totally corrected. Year-long averages for 1986 indicate that only 50 percent of the Gulf Stream, 50 percent of the warm rings, and 25 percent of the cold rings were visible in the satellite IR (Perkins, 1993). Even with a carefully-culled data set, which is composed of time periods with good IR coverage, it was necessary to build composite data over ± 2 days to define the GSNW and ring locations.

3. DEFINITION OF GULF STREAM FRONT

The Gulf Stream front, depending on data type or the application, is defined in several ways. Using SSH and SST, the feature has been defined as the surface NW. From AVHRR imagery data, it is defined as the maximum temperature gradient on the north side of the stream, except for shingles. While using GEOSAT SSH, the surface GSNW is estimated as the northern region of abrupt change in slope to near zero of the SSH that crosses the stream. The estimation error is assumed to be of the order of ± 14 km. Another definition of the feature is the Surface Axis, which is the locus of maximum downstream velocity. The subsurface axis is defined as where the 12°C isotherm crosses 500 m depth.

For practical applications to feature models and OTIS, the often-used criterion is the subsurface NW location, defined as the region where the 15°C isotherm crosses 200m. Since satellite observations can provide only surface definition, the subsurface characterization may be determined in two ways: Use the statistical relationship between the surface and subsurface locations of the fronts; this relationship is derived from empirical data available simultaneously on the front locations at the two levels. Or, employ statistical-dynamical interpolation (data assimilation); this approach dynamically transfers information from observed data to the entire modeling domain.

4. EDGE DETECTION ALGORITHMS

It is well known that the conventional edge derivative operators are essentially high-pass filters that are sensitive to noise and not suitable for analyzing oceanographic satellite images. In ocean circulation applications, the mesoscale fronts and eddies are well defined and continuous. Thus for edge detection from satellite imagery, algorithms must be robust, take advantage of this broad characteristic, and reject fine structure while retaining edge sharpness. However, gridded data from model output are not as noisy, and gradient-based algorithms are able to extract mesoscale features from these data. We will elaborate on this more in Section 9.

4.1 Navy's Cluster Shade Edge Operator

The edge detection algorithm developed by Holyer and Peckinpaugh (1989) is based on cluster shade texture measure, which is derived from the

gray level co-occurrence (GLC) matrix. Although it has been known that the GLC matrix contains edge information (Conners et al., 1984), it had not been used much for the purpose.

Using the GLC matrix, the algorithm computes the 'cluster shade measure', which is essentially the third central-moment of intensity levels. Depending on the distribution of pixel intensity levels, this measure can be positive or negative. Thus, an edge will be indicated from the zero-crossing of this measure. The mathematical formulation of the algorithm has three steps: (i) computation of the GLC matrix; (ii) computation of the cluster shade edge measure; and (iii) determination of the significant zero crossing.

Computation of the GLC Matrix: Its (i,j)th element, $P(i,j|\Delta x, \Delta y)$, is defined as the relative frequency of the pixel-pairs, separated by $(\Delta x, \Delta y)$, one with intensity level i and the other with intensity level j. For an MN array of pixels with $0, 1, \ldots, L-1$ as the levels of of intensity, define a mapping, $f(m,n)$, that assigns intensity level to the pixel (m,n). With this, $P(i,j|\Delta x, \Delta y)$ is defined as

$$P(i,j|\Delta x, \Delta y) = \sum_{m=1}^{M-\Delta x} \sum_{n=1}^{N-\Delta y} A \qquad (1)$$

where

$$A = \begin{cases} \frac{1}{(M-\Delta x)(N-\Delta y)} & \text{if } f(m,n) = i, \text{ and} \\ & f(m+\Delta x, n+\Delta y) = j \\ 0 & \text{otherwise.} \end{cases} \qquad (2)$$

Computation of the the Cluster Shade Measure: This measure, denoted by $S(\Delta x, \Delta y)$, is defined as

$$S(\Delta x, \Delta y) = \sum_{i,j=0}^{L-1} (i + j - \mu_i - \mu_j)^3 P(i,j|\Delta x, \Delta y) \qquad (3)$$

where

$$(\mu_i, \mu_j) = \sum_{i,j=0}^{L-1} (i,j) P(i,j|\Delta x, \Delta y). \qquad (4)$$

Computations are performed in local, overlapping neighborhoods, and the center pixel of the neighborhood is assigned the computed value of $S(\Delta x, \Delta y)$. In other physical applications, image analysis is performed with several $(\Delta x, \Delta y)$ combinations. However, Holyer and Peckinpaugh (1989) found that the edge detection performance of the algorithm is invariant to the choice $(\Delta x, \Delta y)$. Thus, for the sake of simplicity and computational efficiency, they chose $\Delta x = \Delta y = 0$. With this choice, $P(i,j|\Delta x, \Delta y) = 0$ for $i \neq j$, and

$$P(i,i) = P(i), \qquad \text{and } \mu_i = \mu = \sum_{i=0}^{L-1} iP(i). \qquad (5)$$

This gives

$$S(\Delta x, \Delta y) = 2 \sum_{i=0}^{L-1} (i - \mu)^3 P(i). \qquad (6)$$

Determination of Significant Zero Crossings: Because the cluster shade measure is a third moment from the mean, it changes its sign from positive to negative as it goes from a positively-skewed neighborhood to a negatively-skewed one. The values are largest in the vicinity of the GSNW. The values are positive to one side and negative to the other side of the wall, and the transition point from the large positive to large negative value of the measure indicates the GSNW.

To determine significant zero crossings, overlapping 33 pixel neighborhoods are examined in terms of their cluster shade measures. A '0' is assigned to the center pixel if the absolute value of its cluster shade measure is less than a pre-defined threshold value. Otherwise, the neighboring eight pixel values are examined. If the absolute value of any of them is larger than the threshold value and is opposite in sign from the center pixel, a '1' is assigned to indicate an edge. Thus, the entire image is converted into 0s and 1s, the edges being indicated by a two-pixel wide line; it is two-pixel wide because the algorithm detects both positive-to-negative and negative-to-positive transitions of the cluster shade measure values.

This algorithm indicates the need to account for cloud cover in analyzing the AVHRR images. It is suggested that masking procedures could be used for this purpose, but no particular algorithm has been outlined.

4.2 URI Edge Detection Efforts

Evaluation of five edge detection algorithms: Cornillon and Watts (1987) evaluated five different methods of detecting the GSNW. GS maps from 155 AVHRR images were analyzed to locate the northern edge of the GS off Cape Hatteras, North Carolina. One method was the subjective location of the northern edge by the analyst; the other four involved the objective location of the edge by computer using the various statistics of the SST field. Specifically, the quantities considered were: maximum SST gradient (calculated over a 3×3 pixel box), maximum SST (pixel-by-pixel basis), maximum variance (calculated over a 7×7 pixel box), and a change in the skewness of the SST distribution (calculated over a 5×5 pixel box). The resulting locations were compared with the location of the 15 deg isotherm at 200 m (T_{15}) determined from the inverted echo sounders (IESs) moored on the sea floor. The best method that yielded the smallest rms difference from the IES-derived T_{15}, was the subjective one; the surface front was located 9.0 km shoreward of T_{15} with a rms difference of 14.3 km. The best objective technique used skewness of the SST distribution: Each pixel in the image was replaced by the skew of the twenty-five SST values obtained from a 5×5 pixel square centered on the pixel. The skew changes sign when a step in the SST data, such as the GS northern edge, is crossed. The GSNW located from the skew images was found to be 14 km shoreward of T_{15} in the mean with a rms difference of 18.2 km. In general, the more spatial information used, the better was the estimate.

As a part of their AVHRR data analysis at URI, Dr. Cornillon and associates have done a considerable amount of work on developing methodologies to objectively identify features from the SST data, with their applications mainly geared to the estimation of the GS axis. The present URI algorithm is the one developed by Cayula and Cornillon (1992), hereafter referred to as CC92.

URI Edge Detection Algorithm: CC92 developed a sophisticated algorithm to objectively define ocean fronts using AVHRR data. This algorithm is described in some detail in the following, as its objective methodology combined the physical properties of the SST and clouds, and complemented them with statistical methodology. Although edge detection is the main focus of the paper, the problem of cloud detection is also addressed since unidentified clouds can lead to erroneous edge detection.

Cloud Elimination: The removal of cloudy regions is one of the major problems in determining fronts from SST. The algorithm performs a two-dimensional 3×3 median filtering on the original picture and removes the most obvious clouds identified in the following four steps. The first two steps use thresholds on temperature and temperature gradients determined from the fact that the clouds are colder than the ocean and that they are characterized by high gradient magnitudes. The cloudy regions, so determined, are put through two more steps to ensure that the regions are really cloudy. Unlike a real edge, gradient vectors inside the cloudy region are not coherent, yielding a smaller magnitude of the gradient sum as compared to the sum of the gradient magnitudes, i.e., $R = |\sum_{i=1}^{n} \nabla T_i| / \sum_{i=1}^{n} |\nabla T_i|$ is small, where ∇T_i is the temperature gradient at the ith pixel. Thus, the third step classifies the suspected cloudy regions from Steps 1 and 2 as cloudy if $R < .3$ and clear if $R > .7$. For the regions in the range $.3 \leq R \leq .7$, the cloudy regions are bulky, whereas the edges are elongated profiles. Thus, a fourth step classifies the suspected region as cloudy if the aspect ratio (larger eigen value of the spatial covariance matrix divided by the smaller eigen value) is greater than 6.

Histogram Analysis for Frontal Specification: For window level analyses, the CC92 algorithm divides

the total picture into overlapping windows of 32 × 32 pixels and performs the histogram analysis and tests for a two-population hypothesis as follows. Let $h(T)$ be the height of the histogram in the interval denoted by T. Further, divide the data into two parts, $T > \tau$ and $T \leq \tau$, and define

$$J_e(\tau) = \frac{N_1}{N_1 + N_2} S_1(\tau) + \frac{N_2}{N_1 + N_2} S_2(\tau) \qquad (7)$$

where

$$S_i(\tau) = \sum_{\Omega_i} [T - \mu_i(\tau)]^2 h(T)/N_i,$$

with $\{\Omega_1 : T < \tau\}$ and $\{\Omega_2 : T \geq \tau\}$; $N_i = \sum_{T \in \Omega_i} h(T)$ and $\mu_i(\tau) = \sum_{T \in \Omega_i} T h(T)/N_i$. Also, define

$$J_b(\tau) = \frac{N_1 N_2}{(N_1 + N_2)^2} [\mu_1(\tau) - \mu_2(\tau)]^2. \qquad (8)$$

Then the total variance of the window data can be partitioned as:

$$S_{tot} = J_e(\tau) + J_b(\tau)$$

where $J_e(\tau)$ is the within-subgroups variance and $J_b(\tau)$ is the between-subgroups variance. Let $\tau = \tau_{opt}$ maximize $\theta(\tau) = J_b(\tau)/J_{tot}(\tau)$. Assuming Normal distribution,

$$\theta(\tau_{opt}) = 2/\pi \simeq 0.63.$$

Based on the result:

$$\Pr\{\theta(\tau_{opt}) < 0.7\} \simeq 0.99$$

by Duda and Hart (1973), CC92 chose $\theta(\tau_{opt}) = 0.7$ to provide the threshold to check whether there are two different temperature populations in a given window.

Having decided that there are two temperature populations in a window, they again check whether one of them could be fine clouds. This is done in two steps: (1) examine the variability within each subgroup, as the cloudy regions have comparatively a larger variability; (2) perform a correlation test by computing

$$\gamma_X = E(|x - y| - |E(x - y)|), \quad \forall (x, y) \in X \qquad (9)$$

where X is a population. The idea is that if the correlation between neighbors is close to unity, or the variance is small, as would be the case for water, then γ_X will be small. Thus, a threshold, Γ, can be defined so that $\gamma_X > \Gamma$ will classify the region as clouds. Based on their experiments, CC92 chose two thresholds, one for cold ($\Gamma = 4$) and the other for the warm ($\Gamma = 8$).

It is quite possible for the histogram analysis to give a bimodal histogram suggesting two distinct temperature subgroups without having an edge. For there to be an edge separating the two subgroups, each of the two subgroups has to form a connected subset; i.e., for a given pixel that is not close to an edge, the neighboring pixels should belong to the same population. Thus, after eliminating the cloudy region temperatures, CC92 apply a Cohesion Algorithm that is based on three ratios:

$$C_i = \frac{R_i}{T_i}, \; i = 1, 2, \quad C = \frac{R_1 + R_2}{T_1 + T_2},$$

with T_i and R_i are defined as

$$T_i = |\{(x, y) : y \in [\mathcal{N}(x) \cap \mathcal{X}] \forall x \in \Omega_i\}|,$$

$$R_i = |\{(x, y) : y \in [\mathcal{N}(x) \cap \Omega_i] \forall x \in \Omega_i\}|,$$

where $|.|$ defines the cardinality of the set, and $\mathcal{N}(x)$ defines the neighborhood of the pixel, x, as:

$$\mathcal{N}(x_{ij}) = \{x_{i,j+1}, x_{i,j-1}, x_{i-1,j}, x_{i+1,j}\}.$$

In fact, to save computations, they used a modified neighborhood set $\mathcal{N}'(x_{ij}) = \{x_{i+1,j}, x_{i,j+1}\}$. A threshold of 0.92 for C and 0.90 for C_i was chosen so that an edge hypothesis within a window is rejected if either $C < 0.92$ or $C_i < 0.90$. Derivation of these thresholds is based on probability of error formulation.

Having confirmed that a window contains an edge, the last step in the window level processing is to specify the pixels that correspond to the edge. First, define an indicator function that assigns to each pixel within the window a digital count, $I(x) = 0$ if $x \in \Omega_1$, and $I(x) = 1$ if $x \in \Omega_2$. A pixel x is defined as an edge pixel if $I(x) \neq I(y)$, $y \in \mathcal{N}'(x)$.

5. FEATURE LABELING

After the feature edges have been determined, the next step in the automatic feature construction process is to label these edges according to the features present. For instance, in the GS system edges can correspond to several types of features, e.g., warm eddy, cold eddy, North Wall, and South Wall. Unless the labeling is performed with sufficient accuracy, the subsequent feature description will be faulty.

5.1 Relaxation Labeling Algorithm

In the Navy's algorithm, the labeling is performed by a nonlinear probabilistic relaxation process (Krishnakumar et al., 1990a), which requires an initial guess of the probabilities of edge segments belonging to each feature. This first guess is usually available from a previous analysis and moving it forward in time (Holyer and Peckinpaugh, 1990). The relaxation algorithm is composed of two steps. The first step computes *a priori* probabilities from a ground truth data or a recent mesoscale analysis. The second step iteratively updates these *a priori* probabilities until a consistent labeling is achieved. A mathematical formulation by Krishnakumar et al. (1990a) is as follows.

Mathematical Framework: Let $\Lambda = \{\lambda_1, \ldots, \lambda_m\}$ be the set of possible feature labels that can be assigned to pixels $\mathbf{x}$ within a scene. Correspondingly, let $p_\lambda^k(x,t)$ be the probability that the pixel $\mathbf{x}$ is assigned labels λ after k iterations of the relaxation algorithm. The probabilities are allowed temporal dependence so as to take advantage of the temporal continuity of feature evolution.

Step 1: Estimation of *a priori* probabilities: Let $p_\lambda^0(x,t)$ denote the initial probabilities assigned to the pixel $\mathbf{x}(i,j)$ at time t. Then, using the Bayes theorem,

$$p_\lambda^0(x,t) = \frac{p(x,t|\lambda)P(\lambda)}{\sum_\lambda p(x,t|\lambda)P(\lambda)}$$

where $P(\lambda)$ probability of occurrence of the feature λ and $p(x,t|\lambda)$ is the conditional (multivariate) probability density function of a vector $\mathbf{X}$ derived from the physical properties of the pixel $\mathbf{x}(i,j)$, viz, distance and the direction of the pixel $\mathbf{x}(i,j)$ from the origin, gray scale intensity, and the edge magnitude derived using the edge detector algorithm. Thus, $p(x,t|\lambda)$ is specified as

$$p(x,t|\lambda) = (2\pi|\Sigma_\lambda|)^{-\frac{1}{2}} \exp\left\{\frac{-(\mathbf{X}-\mu_\lambda)'\Sigma_\lambda^{-1}(\mathbf{X}-\mu_\lambda)}{2}\right\},$$

where μ_λ and Σ_λ are the mean and covariance matrix of the object λ. Probabilities, $P(\lambda)$ are computed as relative frequencies

$$P(\lambda) = \frac{n_\lambda}{\sum_\lambda n_\lambda}$$

where n_λ are the number of pixels in the object λ.

Step 2: Iterative Updating: Knowing the probabilities, $p_\lambda^k(x,t)$, at iteration k, they are updated as

$$p_\lambda^{k+1}(x,t) = \alpha_\lambda \frac{p_\lambda^k(x,t)(1+q_\lambda^k(x))}{\sum_\lambda p_\lambda^k(x,t)q_\lambda^k(x))} + (1-\alpha_\lambda)p_\lambda(x,t')$$

where $q_\lambda^k(x)$ are called the updating factors, α_λ are temporal weighting functions, and $p_\lambda(x,t')$ is the probability at a prior time $t' < t$. In some cases, the temporal dependence can be removed by setting $\alpha_\lambda = 1$. The updating factors are computed at each iteration as

$$q_\lambda^k(x) = (1/m)\sum_y \sum_{\lambda'} r_{\lambda\lambda'}(x,y)p_{\lambda'}^k(x)$$

where $r_{\lambda\lambda'}(x,y)$ are known as the compatibility coefficients and behave like a correlation coefficient. For example, $-1 \leq r_{\lambda\lambda'}(x,y) \leq 1$; it is positive if λ on $\mathbf{x}$ co-occurs with λ' on y, negative if they frequently do not co-occur, and equality with ± 1 is achieved if the co-occurrence/nonco-occurrence is perpetual. The iterative process is terminated when the difference between two successive probabilities is negligible. For greater detail, see Kittler and Illingworth (1985) where the method of their computation is explained.

The choice of the temporal weighting function is arbitrary and considered to be time varying. In certain situations, the use of this formulation may be problematic; a clear direction towards its choice needs to be formulated. In description of the Navy's expert system, $\alpha_\lambda = 1$ (Krishnakumar et al., 1990b, 1991).

5.2 Contour-Following Algorithm

The URI system does not have a contour labeling algorithm per se. However, as a follow-on to the edge detection step, the system connects the pixels identified as an edge to form a continuous curve to give it a frontal shape. Thus, this algorithm identifies p different contours without assigning any label. This is as opposed to the Relaxation Labeling Algorithm where each pixel, identified as an edge pixel, is assigned a feature label.

The contour following algorithm assigns to the nth pixel of the pth contour the paired value of (n, p). Among the edge pixels detected at the window level that are neighbors of (n, p), the algorithm selects that pixel as $(n + 1, p)$ which affects the least change in the direction of the contour. However, no pixel is added if the direction has to change more than 90 deg in 5 pixels. When no previously-detected edge pixel can be added to the contour, the algorithm examines the ratio $R = |\sum_{i=1}^{n} \nabla T_i| / \sum_{i=1}^{n} |\nabla T_i|$ in a 3×3 pixel window centered on the last contour pixel, where ∇T_i is the temperature gradient at the ith pixel. If $R > .7$, then the algorithm adds to the contour that one pixel from the 3×3 window for which the scalar product of the gradient vector at the pixel point with the gradient vector at the last contour point is the maximum. Because the algorithm relies only on the first neighbors of the last contour edge pixel, it is capable of resolving more than one front in a window. Finally, the algorithm eliminates isolated edge pixels by deleting contours with fewer than 15 pixels.

6. SPATIAL INTERPOLATION ALGORITHMS: DETERMINATION OF THE GULF STREAM LOCATION

Because of cloud cover, the labeled edges provide quite sparse information on the GS front, and it must be filled via interpolation. There are three different approaches at this point. The first one is purely statistical, which is based on empirical information on the mean and the covariance structure of the front. The mean and covariance structure of the feature, derived from climatological records, are combined with the partial observations on the feature for an overall estimation of the feature. The mean provides an anchor, while the covariance structure constrains the estimated solution to conform with the observations. The success of this approach depends on the accuracy of the mean front, the variance of the front at different locations, and the adequacy of the covariance parameterization. The next approach, based on space-time interpolation, overcomes these drawbacks and incorporates the past information. The last approach is that of dynamical interpolation where the sparse information, that may or may not pertain to the front, is assimilated into a dynamical model to provide a synoptic update.

For the statistical approach, four algorithms are reviewed. Not surprisingly, these are based on the well-known techniques of Optimum Interpolation, Empirical Orthogonal Functions, Contour Analysis and Kalman Filtering, which are often used in meteorology and oceanography. The first method, known as the Pathfinder algorithm by Horton (1989), is applied for the objective determination of the surface GSNW. The algorithm is based on the optimum interpolation technique of Bretherton et al. (1976) to interpolate observations on the GS location using the GS climatology as the first guess. The second method is based on the well-known empirical orthogonal functions (EOF) and applied also for the location of the surface GS axis. This technique, described by Molinelli and Flanigan (1987), was originally proposed by Carter (1985). The premise is that the first few CEOF modes incorporate the correlation of the relative location of the fixes along the GS axis. These two algorithms, however, focus on the current epoch of estimation and do not incorporate information from the past (or the future) estimation. The contour-melding procedure by Mariano (1990) utilizes the phase speeds computed from the past and future estimations to perform an overall interpolation of the GSNW position. Chin and Mariano

(1993) take it one step further and cast the estimation problem in terms of a Kalman filter type formulation.

This section is organized as follows. We start with two purely statistical algorithms that combine partial information on a feature with empirically-derived means and spatial/temporal correlations. This is followed by work using a semi-statistical procedure. Dynamic interpolation, or data assimilation, is perhaps the best known technique in this category. It combines output of a numerical ocean model with observations that may not necessarily be on the feature. The feature is then extracted, using some specified formulation of the feature definition. OFI work using AVHRR data, done by Cornillon and colleagues, pertains to a different type of semi-statistical approach in that it exploits the physical characteristics of the variable underlying the feature, and uses statistics to establish thresholds to test the sequential hypotheses to extract features.

6.1 The Pathfinder Algorithm

The Pathfinder algorithm is based on the mean and covariance concept. It converts observed (longitude, latitude) positions into (downstream, cross-stream) anomalies relative to a mean path. Then the approach assumes that the GS meanders, in terms of cross-stream anomalies along the mean path, form a second-order stationary process, i.e., the covariance between two cross-stream anomalies is a function of the downstream distance between them. The implementation of the algorithm is described in terms of the objective analysis technique of Bretherton et al. (1976). This OI technique is used to estimate the GS path from a limited number of observations on the GS positions with varying ages.

The brief description given below provides elaboration of the statistical details of the method.

Let (x_j, y_j), $j = 1, \ldots, n$ be given observations on the GS axis, where x_j is the downstream anomaly and y_j is the measurement on jth cross-stream anomaly η_j. The problem is to estimate $\eta = \eta(x)$ for a specified downstream anomaly x. Then y_j can be expressed using a simple statistical model:

$$y_j = \eta_j + \epsilon_j, \quad j = 1, \ldots, n \tag{10}$$

where statistical expectation of η_j is zero, i.e., $\mathcal{E}(y_j) = 0$. The observed GS positions are contaminated by random measurement errors, ϵ_j, that are uncorrelated with one another, i.e., $\mathcal{E}(\epsilon_j \epsilon_k) = \delta_{jk}\sigma_\epsilon^2$, with δ_{jk} being the Kronecker's Delta function and σ_ϵ^2 the measurement error variance. The measurement errors are uncorrelated with GS position anomalies, i.e., $\mathcal{E}(\epsilon_j \eta_k) = 0$. The statistical model is completed with a specification of the covariance between various observation pairs in terms of the covariance matrix $\mathbf{A} = (A_{ij})$ where

$$\begin{aligned} A_{ij} &= \mathcal{E}(y_i y_j) = \mathcal{E}(\eta_i \eta_j) + \sigma_\epsilon^2 \delta_{ij} \\ &= C_{ij} + \sigma_\epsilon^2 \delta_{ij}. \end{aligned}$$

The covariance, C_{ij}, is a function of the GS spreads (variances) σ_i and σ_j at downstream distances x_i and x_j and the correlation function, $c(x_i, x_j)$. Thus,

$$C_{ij} = \sigma_i \sigma_j c(x_i, x_j).$$

Let the covariance of $\eta = \eta(x)$ with each η_j be given by

$$C_{xj} = \mathcal{E}(\eta(x)\eta_j).$$

With this setup, we can estimate $\eta(x)$ as a linear function of the observations:

$$\hat{\eta}(x) = \sum_{j=1}^{n} \alpha_j y_j, \tag{11}$$

where the coefficients α_j are derived from a least squares formulation as follows. Let $\mathbf{Y} = (y_1, \ldots, y_n)'$, $\mathbf{C}(x) = \mathbf{C} = (C_{x1}, \ldots, C_{xn})'$, where $'$ represents matrix transposition. Then, according to the least squares formulation, we minimize

$$\begin{aligned} \mathcal{E}(\eta - \hat{\eta})^2 &= \mathcal{E}(\eta(x) - \boldsymbol{\alpha}'\mathbf{Y})^2 \\ &= \mathcal{E}[\eta(x)^2 - 2\boldsymbol{\alpha}'\mathbf{Y}\eta(x) + \boldsymbol{\alpha}'\mathbf{Y}\mathbf{Y}'\boldsymbol{\alpha}] \\ &= c_{xx} - 2\boldsymbol{\alpha}'\mathbf{C} + \boldsymbol{\alpha}'\mathbf{A}\boldsymbol{\alpha} \\ &= [\boldsymbol{\alpha} - \mathbf{A}^{-1}\mathbf{C}]'\mathbf{A}[\boldsymbol{\alpha} - \mathbf{A}^{-1}\mathbf{C}] \\ &\qquad + C_{xx} - \mathbf{C}'\mathbf{A}^{-1}\mathbf{C}. \end{aligned} \tag{12}$$

Note that the last two terms in eq. (12) are independent of α, and the first term involving α is a positive definite quadratic form in the matrix A. Thus, the minimum is obtained by setting

$$\alpha = \mathbf{A}^{-1}\mathbf{C},$$

and the estimation error is given by

$$\begin{aligned}\mathcal{E}(\eta(x) - \alpha'\mathbf{Y})^2 &= C_{xx} - \mathbf{C}'\mathbf{A}^{-1}\mathbf{C} \\ &= C_{xx} - \sum_{r,s=1}^{n} C_{xr}C_{xs}A^{rs}. \quad (13)\end{aligned}$$

where A^{rs} is the rsth element of $\mathbf{A}^{-1}$. This derivation is similar to that in Bretherton et al. (1976), but simpler due to the use of the matrix notation. Thus, $y(x)$ for a specified x is estimated as:

$$\begin{aligned}\hat{y}(x) &= \alpha'\mathbf{Y} \\ &= \mathbf{C}'\mathbf{A}^{-1}\mathbf{Y} \\ &= \sum_{j=1}^{n} C_{xj}\left(\sum_{k=1}^{n} A^{jk}y_k\right) \quad (14)\end{aligned}$$

In both Horton (1989) and Bretherton et al. (1976), eq. (14) has been written as:

$$\hat{y}(x) = \sum_{j=1}^{n} C_{xj}\left(\sum_{k=1}^{n} A_{jk}^{-1}y_k\right).$$

This unconventional notation is liable to cause confusion, since A_{jk}^{-1} is interpreted as $1/A_{jk}$ and not as A^{jk}.

Horton (1989) makes the basic assumption of stationarity of covariance in terms of the downstream coordinate x. For two points at downstream distances x and r, he formulated his equation (14) in terms of a prescribed correlation function, $c_{xr} = c(|x - r|)$, given by:

$$c_{xr} = \cos(2\pi|x - r|/w_1)\exp(-|x - r|^{1.5}) \quad (15)$$

where $w_1 = 450$ km is the wavelength and Δ is the decay variable, $= .00032001$ km$^{-3/2}$. Thus, $C_{xr} = \sigma_x\sigma_r c(|x - x_r|)$, where σ_x^2 is the variance of the meander at the downstream coordinate x.

For further details on the operational implementation of the model, see Horton (1989), where he suggests ways of using old observations. GS front location estimation errors are due to several sources; some of them are: observation error variance, variance of the meander envelope around the mean front location, the assumption of stationary covariance and the choice of the corresponding correlation function. Based on his simulation experience, Horton (1989) concludes that:

- The mean path errors are not well understood. The variance of the mean path error might be typically about 25 percent of the meander envelope.
- The effect of the mean path errors can be reduced by modifying the correlation function used in the optimum interpolation, which lets the observations modify the mean path.
- Using the optimum interpolation method, the errors in the interpolated paths were below 50 km, even with observational gaps of up to several degrees longitude. However, he conjectured that the inadequate sampling, coupled with atypical meanders such as ring-formation events, might produce errors two to three times as great.

6.2 Complex Empirical Orthogonal Function Algorithm for the Gulf Stream Path

The empirical orthogonal function (EOF) approach is another statistical approach commonly used in the literature to capture the overall correlation of a space-time feature in a few vectors. These vectors are the eigen vectors of the empirically-estimated covariance matrix of the feature and are referred to as the EOFs of the feature. To construct a specific synoptic realization of the feature, one simply computes a weighted sum of these EOFs, where the weights are given by the EOF 'amplitudes' corresponding to the feature realization. Thus, the EOF approach involves two steps. One is to derive the EOFs from the empirically-estimated covariance matrix of the feature. This step is performed once for all subsequent construction (estimation) of the features. The second step requires converting partial

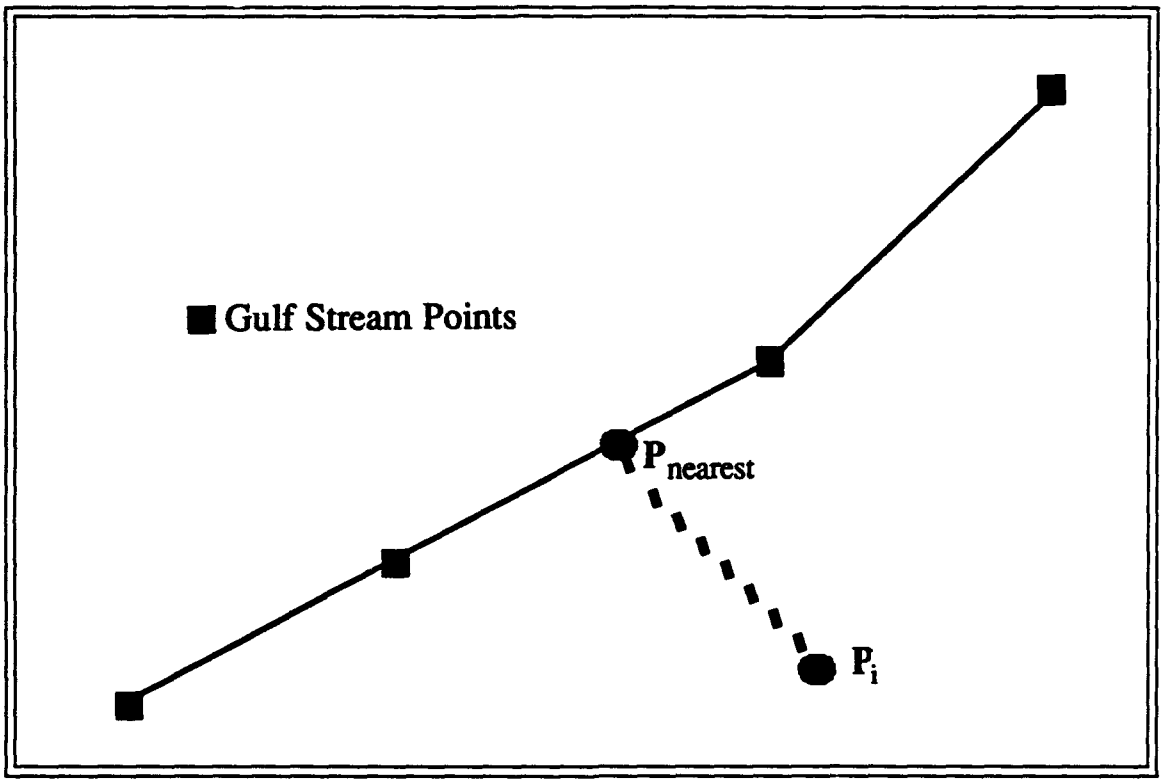

Figure 1. CEOF optimization geometry; P_i is an observation and $P_{nearest}$ is its projection on lineraly segmented GS path constructed at an earlier step.

observations on a feature realization into EOF amplitudes so that the weighted sum of the EOFs can be computed to derive the entire realization. This step is repeated each time a feature realization has to be constructed. Carter (1985) proposed the concept using complex EOFs (CEOFs) to describe the GS path. Molinelli and Flanigan (1987), hereafter referred to as MF87, followed it up by developing an algorithm that successively updates the CEOF analyses with a partial set of observations to yield a new fix of the GS axis. In this formulation, a location (x, y)= (longitude, latitude) is represented as a complex number $w = x + iy$. Thus, $w_j = x_j + iy_j$ are the locations along the Gulf Stream axis at equal spatial distance intervals, so that the vector $\mathbf{w} = (w_1, \ldots w_N)'$, $'$ indicating matrix transposition, defines a discrete representation of the Gulf Stream. Let $\Sigma = \langle w_i w_j^* \rangle$, where * indicates complex conjugate and $\langle\rangle$ denotes ensemble average. Let $\mathbf{e}_j, j = 1, \ldots, n$ be the eigen vectors of Σ with λ_j as the corresponding eigen values. Since Σ is Hermitian, the eigen values λ_j are real; however, the eigen vectors are complex. With this, we can define rotated variables (complex amplitudes)

$$c_k = \mathbf{e}_k^* \mathbf{w} \tag{16}$$

where $\mathbf{e}_k^*$ is the complex conjugate transpose of $\mathbf{e}_k$. The original discrete GS representation, $\mathbf{w}$, can be recovered from c_k as the weighted sum of the EOFs:

$$\mathbf{w} = \sum_{k=1}^{N} \mathbf{e}_k c_k = \mathbf{E}\mathbf{c}, \tag{17}$$

where $\mathbf{E} = \mathbf{E}_N = (\mathbf{e}_1, \ldots \mathbf{e}_N)$ and $\mathbf{c} = c_N = (c_1, \ldots, c_N)'$.

At this time, we reiterate some points pertaining to the GS estimation using the CEOFs:

- The EOFs, represented by the eigen vectors $\mathbf{e}$, are obtained from the statistical population of the

Gulf Stream axis, and thus, entail the overall correlation structure between various locations of the Gulf Stream axis;

- However, the amplitudes c_k represent characteristics of an individual GS realization and vary from one GS realization to another.

- In general, the overall variability of the system can be explained by a small number, say n, of modes. Thus, a GS realization w in eq. (17) can be approximated as the weighted sum of the dominant EOFs:

$$\mathbf{w} \simeq \sum_{k=1}^{n} \mathbf{e}_k c_k = \mathbf{E}_n \mathbf{c}_n, \tag{18}$$

- We observe from eq. (18) that $\mathbf{E}_n$ acts as a 'basis set' of vectors, and a GS realization is obtained as a linear combination of the basis set. Writing $c_k = a_k \exp(i\phi_k)$, we note that weighting with a_k results in an amplification as well as a rotation of the EOF vector, $\mathbf{e}_k$.

MF87 solved the problem of estimating a GS realization from only a partial information using the CEOF formulation. For this, the partial information is mapped onto complex amplitudes, $\mathbf{c}_n = (c_1, \ldots c_n)^T$, so that the realization w could be constructed using eq. (18). The MF87 implementation was based on empirical data sets derived from 84 realizations of the Gulf Stream axis, interpolated at $N = 132$ equidistant points with 10 km spacing along the GS axis. They could describe the Gulf Stream shapes with as few as $n = 10$ modes, accounting for 99 percent of the variability. The root mean square difference between the 132 estimated and the empirical GS fixes, with $n = 10$ using eq. (18), was ~ 6 nmi.

A nonlinear least squares, gradient-search algorithm was used to map the partial observations on the GS axis onto the complex amplitude vector $\mathbf{c}_n$. The approach is to start with a set of $c_i, i = 1, \cdots, n$ based on a well-defined snapshot of GS, and then optimally adjust the c_i until the resulting w deviates from the few available GS fixes in a least squares sense. Mathematically, the formulation is as follows.

At any time, let $\mathbf{p}_j, j = 1, \cdots, K$ be partial information on the GS axis in terms of K position fixes. An individual $\mathbf{p}_i$ could be from any source, including IR and SSH. Then according to the least squares criterion, we would like to determine a GS, $\mathbf{w} = \sum_{k=1}^{n} \mathbf{e}_k c_k$, that minimizes

$$\mathbf{X}^2 = \sum_{i=1}^{K} \sigma_i^{-2} |\mathbf{p}_i - \mathbf{p}_{i\mathbf{w}}|^2, \tag{19}$$

where σ_i^2 is the position error variance for $\mathbf{p}_i$, and $\mathbf{p}_{i\mathbf{w}}$ is the projection of the observed position $\mathbf{p}_i$ on the to-be-determined discrete GS representation w; see Fig. 1. The details of the minimization procedure used are standard (see Bevington, 1969), and are thus omitted.

The minimization of $\mathbf{X}^2$ in eq. (19) is nonlinear in the parameters $c_i, i = 1, \cdots, n$, and thus requires their initial guesses. These guesses are obtained by substituting in eq. (16) a pre-existing discrete GS realization $\mathbf{w}_0$. Since the above minimization requires the estimation of $2n$ parameters, corresponding to the real and imaginary parts of $\mathbf{c}_n$, we must have $K \geq n$. The MF87 study indicates that for a GS axis estimation, the number of fixes from SSH and AVHRR is typically in the 25 to 75 range, and thus quite adequate for estimation purposes.

According to the simulation results of MF87, this procedure provides an accuracy of 30 nmi, the same as obtained in manual analyses performed by WSC. However, because the computer optimization is automated, it minimizes manual analysis.

6.3 CONTOUR ANALYSIS

Mariano (1990) came up with a contour analysis approach for melding different analyses of geophysical fields, which he adapted for interpolating the GSNW position from gappy information. He argued that the combining of two or more different fields using the usual weighted averaging or least

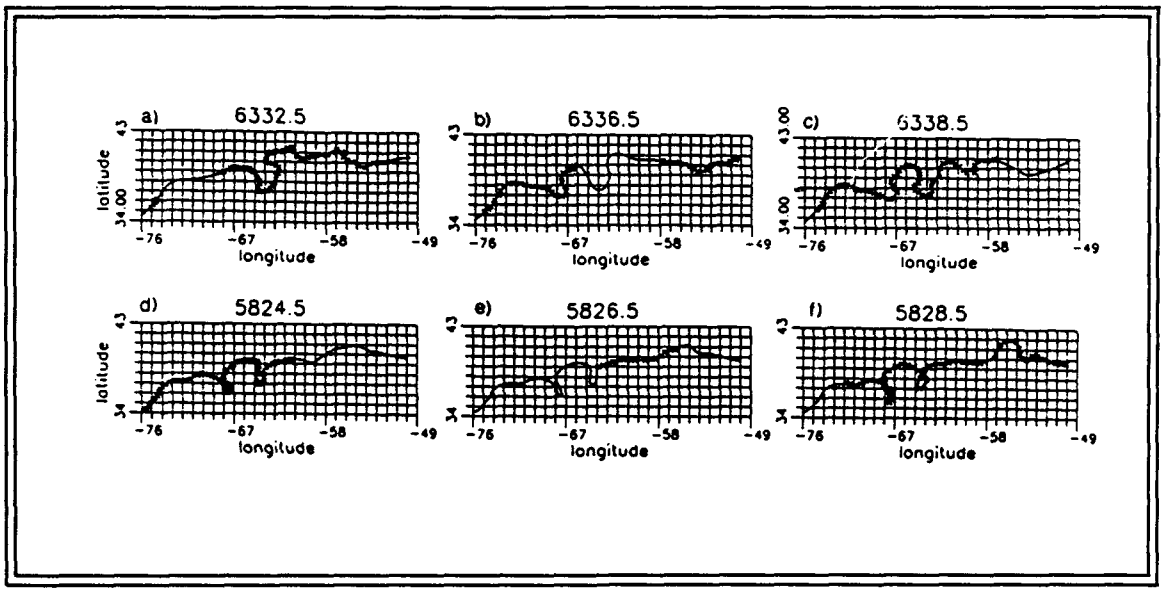

Figure 2. Example of contour analysis interpolation of GSNW (Adapted from Mariano, 1990)

squares approach would tend to smear the information on the features. To alleviate this problem, he proposed contouring the various analyses and melding the positions of the features as specified by contours, rather than averaging the fields. This approach has the distinct advantage of retaining the shapes of the features while appropriately adjusting the amplitude and phase information. For a formal but brief description of the Contour Analysis approach, consider the melding of two fields characterized by sets, $C_i, i = 1, 2$, of contours such that

$$C_i = \{C_i(j)\},$$

where j represents the contour number, and melding is to be performed by combining corresponding contours in the two fields. Let two such corresponding contours be specified by C_1 and C_2, where the contour index j is dropped for notational convenience. Then C_i are represented by longitude, latitude positions as

$$C_i = \{(x_{ik}, y_{ik}), k = 1, 2, \cdots, n_i\}. \qquad (20)$$

At this stage, there is a need to set up a correspondence between C_1 and C_2 in terms of the geophysical feature to be extracted. The correspondence is established by selecting points located at the same fraction of the arc lengths along each contour. Mariano's implementation of this correspondence is as follows:

- Compute arc length: For each contour, start with the original sets of points $C_i : (x_{ik}, y_{ik})$, $k = 1, \cdots, n_i$, and define arc lengths as follows. Let $\Delta x_{ik} = (x_{ik} - x_{i(k-1)})$ and $\Delta y_{ik} = (y_{ik} - y_{i(k-1)})$. Then, $\Delta S_i(k) = (\Delta x_{ik}^2 + \Delta y_{ik}^2)$ is the arc length between points $(x_{i(k-1)}, y_{i(k-1)})$ and (x_{ik}, y_{ik}). The arc length corresponding to the lth point (from the first point) is given by

  $$S_{il} = \sum_{k=2}^{l} \Delta S_i(k);$$

  The total arc length for the ith contour is denoted by S_i.

- Set up correspondence between C_1 and C_2: This correspondence is set up in two steps: (1) First, for each contour, C_i, fit separate cubic splines to x_{ik} and y_{ik} as a function of the arc length, S_{ik}. (2) From the splines, then interpolate at N (the same number for the two contours) of new points, (X_{ik}, Y_{ik}), $k = 1, \ldots, N$ at equal arc length intervals, $\Delta S_i = S_i/N$. The choice of arc length

as the independent variable permits melding of multivalued features with an appropriate phase.

- With this at hand, the melded contour is calculated as;

$$(\tilde{X}_k, \tilde{Y}_k) = \left(\sum_{i=1}^{2} w_{ik} X ik, \sum_{i=1}^{2} w_{ik} Y ik \right), \qquad (21)$$

for $k = 1, \cdots, N$, where the weight w_{ik} may be chosen proportional to the inverse of the error-variance assigned to each position, such that $w_{1k} + w_{2k} = 1$.

Mariano applied the above contour melding technique to incomplete, time-varying fields to perform space-time interpolation of the GSNW for 824 cases. The SST data from the AVHRR were mapped to a common coordinate system and composited into two-day groups at the URI, retaining the warmest pixel out of approximately ten satellite passes. The GSNW position was then hand digitized.

Due to cloud cover, the resulting data sets from the above operations suffered from several spatial and temporal gaps that needed to be filled. To demonstrate, Fig. 2 adapted from Mariano (1990) shows two examples of filling gaps in the the GSNW positions using contour analysis interpolation. Fig. 2b shows the hand digitized GS region on Day 6336.5 with gaps between 66° and 58°W. The first step to fill these gaps was to find, in the immediate past (Day 6332.5, Fig. 2a) and the future (Day 6338.5, Fig. 2c), GSNW records which provided coverage for the gappy area under consideration. For a proper application of the contour analysis algorithm, the two records were propagated to a common analysis time. A phase speed was computed by averaging the propagation speed of the local maximum and minimum between the past and future time assuming a dominant east-west propagation speed. The latitudes were propagated forward for the past and backward for the future. With the time synchronization done, the contour analysis fitted cubic splines to latitudes and longitudes of the 'past' and 'future' records as a function of the arc lengths. These splines were interpolated to create the new data sets at equal arc lengths, which were then averaged according to eq. (21) to obtain the fully-interpolated data sets. The weights, w_{ik} were taken to be inversely proportional to the time between the present gap and the time of the past and future data. Thus for the past, $w_{1k} = 1/3$, and for the future, $w_{2k} = 2/3$. Fig. 2d–f show another example of similar interpolation.

Summarizing the Contour Analysis approach to interpolate the gappy areas of the GS positions we note:

- The GSNW is a multivalued phenomenon which has been difficult to resolve. Mariano's approach is quite ingenious in fitting splines to latitude and longitudes as functions of an independent variable, arc length.
- The approach combines the phase and amplitudes of two sets so as to preserve an appropriate shape.
- Mariano (1988) has applied this approach to create an atlas of 824 GSNW positions with quite satisfactory results.
- Algorithm performance deteriorates for those cases involving ring-births or strong ring-stream interactions.
- Algorithm performance can be improved by employing two-dimensional phase speeds and also by using better ways to calculate these phase speeds.
- In simulation experiments performed by Mariano (1990), he found the interpolation error was of the order of 10 km.
- The largest interpolation errors (50-80 km) were found in the meander amplitudes in the vicinity of 58°W in each curve.

6.4 Optimal Space-Time Interpolation

Mariano's approach of using the arc length as the independent variable to interpolate the GS

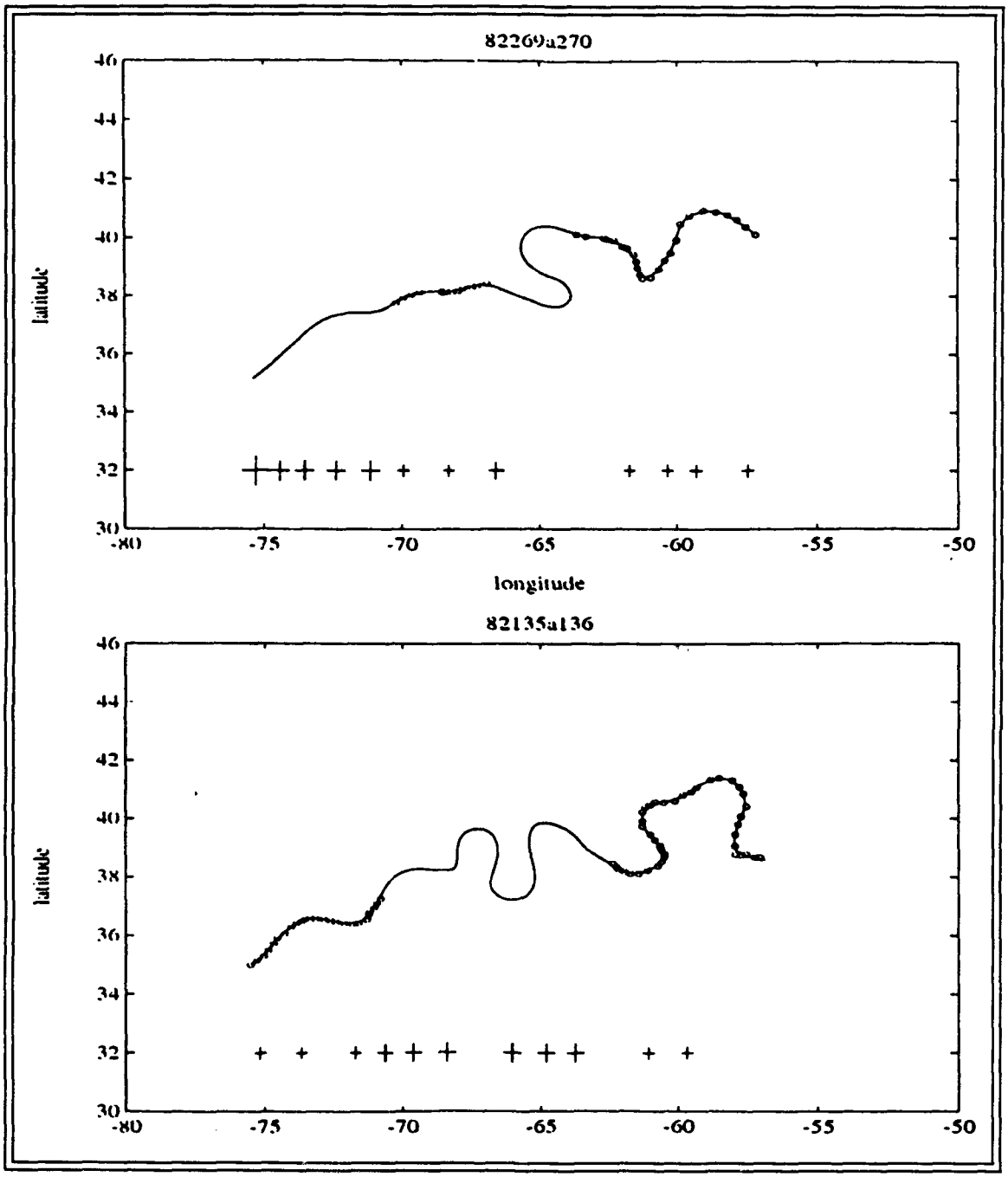

Figure 3. Examples of complex GS meanders in 'S' and 'Ω' shapes. Estimation errors are indicated by the size of '+' signs (Adapted from Chin and Mariano, 1993)

path was a major step in being able to resolve complex and multivalued meanders of 'S' and 'Ω' shapes. It also introduced the use of past and future observations in computing the GS path at the present time. However, the approach was heuristic. Chin and Mariano (1993), referred to as CM93 in the following, enhanced the Mariano approach by formalizing the concept via a Kalman

type 'predictor-corrector' approach, while retaining the arc length concept. Let $p(s,t) = [x(s,t), y(s,t)]'$ be the true GS contour locations at time t and arc length s relative to some reference point. The arc length s of p is discretized so that the final GS is represented by a vector $\mathbf{p}(k)$ whose ith element p_i corresponds to arc length $s_i = i\Delta s$ at time $k\Delta t$. Since $\mathbf{p}$ is yet to be estimated, there is no knowledge about its arc length. However, there is no confusion as far as notation is concerned. Let $\tilde{\mathbf{p}}_{ik}, i = 1, \cdots, m_k$ be the observation points digitized from the kth SST image. It is assumed that the discretization is fine enough such that, up to some quantization error, the arc length, $\tilde{\sigma}_i$, associated with the observed data $\tilde{\mathbf{p}}_{ik}$ corresponds as $\tilde{\sigma}_i = j\Delta s$ for some j. Then their space-time interpolation is obtained by that $\mathbf{p}(s,t)$ which minimizes

$$\begin{aligned}&\sum_{k=1}^{K}\sum_{i=1}^{m(k)}\nu_i(k)\|\tilde{\mathbf{p}}_{ik} - p(s_{ik}, k\Delta t)\|^2 \\ &+ \int_0^T \int_C \left[\alpha_1\|\frac{\partial p}{\partial s}\|^2 + \alpha_2\|\frac{\partial^2 p}{\partial s^2}\|^2\right] dsdt \qquad (22)\\ &+ \int_0^T \int_C \left[\beta_1\|\frac{\partial p}{\partial t}\|^2 + \beta_2\|\frac{\partial^2 p}{\partial t^2}\|^2\right] dsdt\end{aligned}$$

where the time variable is discretized as $t = k\Delta t$, $k = 1, \cdots, K$, and ν_i are the weights indicating confidence in the observations; the constants α_1 and α_2 control spatial continuity (tension) and linearity (smoothness); and similarly, the constants β_1 and β_2 control the temporal constraint and linearity. Equation (22) can be interpreted in terms of Kalman filter-based equations as:

$$\begin{pmatrix}\mathbf{p}_k\\ \mathbf{p}_{k+1}\end{pmatrix} = \begin{pmatrix}\mathbf{I} & \mathbf{0}\\ -\mathbf{I} & 2\mathbf{I}\end{pmatrix}\begin{pmatrix}\mathbf{p}_{k-1}\\ \mathbf{p}_k\end{pmatrix} + \begin{pmatrix}\mathbf{w}_{1k}\\ \mathbf{w}_{2k}\end{pmatrix} \qquad (23)$$

and

$$\begin{pmatrix}\mathbf{q}_k\\ \mathbf{0}\\ \mathbf{0}\end{pmatrix} = \begin{pmatrix}\mathbf{H}(\mathbf{p}_k, k)\\ \mathbf{S}_1\\ \mathbf{S}_2\end{pmatrix}\mathbf{p}_k + \begin{pmatrix}\mathbf{v}_{Hk}\\ \mathbf{v}_{1k}\\ \mathbf{v}_{2k}\end{pmatrix} \qquad (24)$$

where $\mathbf{q}$ is the observation vector and $\mathbf{H}$ is the data-estimate correspondence operator with its (i,j)th element defined as

$$h_{ij} = \begin{cases}1 & \text{if } \tilde{s}_i = j\Delta s\\ 0 & \text{otherwise;}\end{cases}$$

$\mathbf{S}_1$ and $\mathbf{S}_2$ are matrices of first and second order operators; $\mathbf{w}_i$ are independent, zero-mean, Gaussian error vectors with $\beta_i^{-1}\mathbf{I}$ as covariance matrices; and $\mathbf{v}_H$, $\mathbf{v}_1$ and $\mathbf{v}_2$ are zero-mean Gaussian random error vectors with covariance matrices $\mathrm{diag}(\nu_1^{-1}, \cdots, \nu_m^{-1})$, $\alpha_1^{-1}\mathbf{I}$, and $\alpha_2^{-1}\mathbf{I}$.

Writing $d_k = \mathbf{p}_{k+1} - \mathbf{p}_k$, then eq. (23) can be rewritten as

$$\begin{pmatrix}\mathbf{p}_k\\ \mathbf{d}_k\end{pmatrix} = \begin{pmatrix}\mathbf{I} & \mathbf{I}\\ \mathbf{0} & \mathbf{I}\end{pmatrix}\begin{pmatrix}\mathbf{p}_{k-1}\\ \mathbf{d}_{k-1}\end{pmatrix} + \begin{pmatrix}\mathbf{w}_{1k}\\ \mathbf{w}_{2k}\end{pmatrix} \qquad (25)$$

The Kalman formalization provided by eqs. (24) and (25) is the same in spirit as that of Mariano (1990), except that it employs two-dimensional phase speeds and, in addition, is optimal in the least squares sense. These equations can be solved by procedures given in Gelb (1974) and Lewis (1986). However, there is an inherent difficulty in that the spatial coordinates of the digitized points are unknown; thus the observation-data correspondence matrix $\mathbf{H}$ is also undefined. Also, the origin of the spatial coordinate s is difficult to define. The arc length coordinates, s_i must be determined concurrently as the contours are interpolated.

The above problems are alleviated by taking an "adaptive approach where best predictions of the GSNW contour data given time k are used to estimate the positions, i.e., arc length indexes, $s_i(k)$, of the measurement along the contour". An iterative procedure is employed where for each time index k, $s_i(k)$ and $\mathbf{p}(k)$ are estimated alternately using the best guess of the other. The observation-data correspondence matrix $\mathbf{H}(\mathbf{p}_k, k)$ in eq. (24) is evaluated as the $\hat{\mathbf{H}}(\mathbf{p}_f(k-1), k)$ in the forward filter and as $\hat{\mathbf{H}}(\mathbf{p}_b(k+1), k)$ in the backward filter where $\hat{\mathbf{p}}_f(k)$ and $\hat{\mathbf{p}}_b(k)$ the forward and backward filtered estimates. In other words, a correspondence is set up for the observations at time k with the curve predicted to time k from an estimated contour at time $k-1$. The iteration procedure was terminated after convergence or after a fixed number of iterations. Because of gaps in measurements at any time k, the estimates of the

previous frame, p_{k-1}, are often the best guess of the general shape at time k.

The correspondence referred to above is performed 'hierarchically', first using large-scale 'features', followed by smaller, local and then using inflections of the curves. Based on the interpolation of 150 frames, CM93 conclude the following:

- The algorithm, in general, is quite successful in reconstructing features like the 'S' and 'Ω' shapes. Fig. 3 is an example of two such realizations.
- The Kalman-type formulation provides the errors of estimations as shown in Fig. 3.
- The algorithm is unable to resolve some fast movements of the meanders and to detect transformations of the meanders into rings.
- The algorithm is dependent on the digitization process of the GS positions using SST data, which in itself is quite a laborious process. (The work of Cayula and Cornillon (1992) should alleviate this problem to some extent).
- 'The present-day pattern recognition and matching algorithms have yet to realize flexibility and sensitivity of trained personnel'.

6.5 Dynamic Interpolation

The dynamic interpolation approach combines dynamic information from a numerical model with the actual observations on the thermo-dynamic structure. It is not necessary that the observations be on the feature to be extracted. The information content in an observation is first spread in the neighboring areas statistically using spatial and temporal covariance functions, and then communicated dynamically via numerical integration. The three-dimensional numerical model output is then subjected to a feature detection algorithm.

Briefly, let T be the true state of the ocean, which is to be estimated by combining the model output, $\mathbf{T}_m$, and observations $\mathbf{T}_o$. The vectors T and $\mathbf{T}_m$ are N-vectors defined on the model grid, $\mathcal{G}_m$; the observation vector, $\mathbf{T}_o$ is an M-vector defined on the observation grid $\mathcal{G}_o$. Usually, $M << N$, and $\mathbf{T}_o$ alone cannot provide an adequate representation of T. Thus, assimilation is performed, resulting in an estimate on $\mathcal{G}_m$ to provide initial conditions for the numerical integration of the model equations.

We assume there exists a mapping $\mathbf{D}(\mathcal{G}_m) = \mathcal{G}_o$. Then $\mathbf{T}_o$, the true state of the ocean at the observation grid, can be written as $\mathbf{T}_o = \mathbf{D}(\mathbf{T})$. Often D is assumed to be a linear mapping so that:

$$\mathbf{T}_o = \mathbf{DT}. \tag{26}$$

The assumption here is that both the model values and the observational data are unbiased estimators of the true state of the ocean, and that the optimal combination of the two will lead to an estimator of T, which has a smaller error variance than either of the two. Under the unbiasedness assumption, we can write the following linear model:

$$\begin{pmatrix} \mathbf{T}_m \\ \mathbf{T}_0 \end{pmatrix} = \begin{pmatrix} \mathbf{T} \\ \mathbf{DT} \end{pmatrix} + \begin{pmatrix} \mathbf{e}_m \\ \mathbf{e}_0 \end{pmatrix} \tag{27}$$

where $\mathbf{e}_m$ and $\mathbf{e}_o$ are vectors of zero mean random errors in the model output and observations, with Σ_m and Σ_o as their respective covariance matrices. It is reasonable to assume that the errors in $\mathbf{T}_o$ and $\mathbf{T}_m$ are statistically independent. Then, the least squares solution to the true state T is obtained by minimizing the quadratic functional:

$$\begin{aligned} Q = &(\mathbf{T}_m - \mathbf{T})'\Sigma_m^{-1}(\mathbf{T}_m - \mathbf{T}) \\ &+ (\mathbf{T}_o - \mathbf{DT})'\Sigma_o^{-1}(\mathbf{T}_o - \mathbf{DT}) \end{aligned} \tag{28}$$

where the prime indicates matrix transposition. Navon and Liegler (1987) describe several efficient procedures to affect the above minimization.

The estimate, $\hat{\mathbf{T}}$, of the true state of the ocean, T, obtained from the above minimization procedure is referred to as dynamical interpolation. It reflects the information content of the dynamical model and the observations. Appropriate algorithms can be used for OFI. The modelers in DAMEE-GSR used the 15 deg isotherms at 200 m depth algorithm on dynamically interpolated output to derive the GSNW (Perkins, 1993).

6.6 Eddy Detection

Eddy detection from the labeled edges is performed in either circular or elliptical shapes. The algorithm used in the Navy's SAMAS is the Hough transform (Lybanon and Holyer, 1991), which can be used to detect lines and curves in pictures. It essentially involves computing convolutions of the labeled edges with various binary kernels representing a possible shape that can be ascribed to the labeled edges. The curve selected is the one for which the kernel shape optimizes the convolution. Thus, if circles are to be assigned as eddy shapes to the labeled edges, then the kernel library of possible shapes consists of circles of 1s of possible radii. Duda and Hart (1972) provide a general description of the circular Hough transform. The solution by this procedure is equivalent to the least mean squares solution when the edge pixels are assumed to be contaminated with identically and independently distributed random noise.

Szczecchowski (1991) proposed the Marr-Hildreth operator as an edge detector. The Marr-Hildreth operator performs the convolution

$$E(x,y) = \nabla^2 G(r) * I(x,y)$$

where ∇^2 is the Laplacian operator, * represents the convolution, $G(r)$ is the Gaussian function in polar coordinates

$$G(r) = \frac{1}{\pi} \exp\left(-\frac{r^2}{2\sigma^2}\right)$$

and $I(x,y)$ is the two-dimensional image intensity. To obtain a better delineation of the eddy curve, convolutions are performed at more than one value of σ. The zero-crossings of $E(x,y)$ determine the eddy. The eddy center is determined from the mean of the pixel locations enclosed within the curve. The Marr-Hildreth operator possesses several desirable properties: It attenuates high frequencies; there is only one free parameter, which is the scale parameter, σ; no thresholds are needed for edge detection; and, the resultant edges form a closed continuous curve. For further details of the algorithm, see Szczecchowski (1991).

Other algorithms for circle detection that optimize some distance function between the center and the edge pixels have been considered for eddy detection. The Thomas-Chan algorithm minimizes a theoretical, area-based error function (Thomas and Chan, 1989) to give an explicit formula for the center and radius of the circle in terms of the edge-pixel coordinates. The Landau (1987) algorithm is an iterative algorithm which minimizes the mean distance between the edge-pixels and the center. The Albano (1974) fits a general conical curve using the least squares formulation. Peckinpaugh and Holyer (1994) performed a relative evaluation of these and the Hough transform circle detection algorithms; the Thomas-Chan algorithm provided the best overall accuracy in the tested examples.

7. TWO GULF STREAM IDENTIFICATION SYSTEMS

At present, the surface NW location is determined subjectively by the Naval Oceanographic Office Warfighting Support Center (WSC) using predominantly AVHRR data. As discussed earlier, this operation may be greatly hampered because of cloud cover, which conceals ocean features. In cloud-covered areas, the operator must make a completely subjective estimate of frontal location, usually based on its last known position. This procedure, in addition to being ponderous and time consuming, is quite subjective. There obviously is an urgent need to develop an automatic and objective procedure to perform this tedious but important task. The Navy has taken a lead in this task and, in a systematic manner, identified and constructed various components of feature identification as a part of their Semi-Automated Mesoscale Analysis System. Included here also is the URI system. Although it is not as up-to-date as SAMAS, the URI algorithm development seems to be headed in the direction of a complete system. The following, although somewhat repetitive, is provided as brief and up-to-date information on the two complete systems.

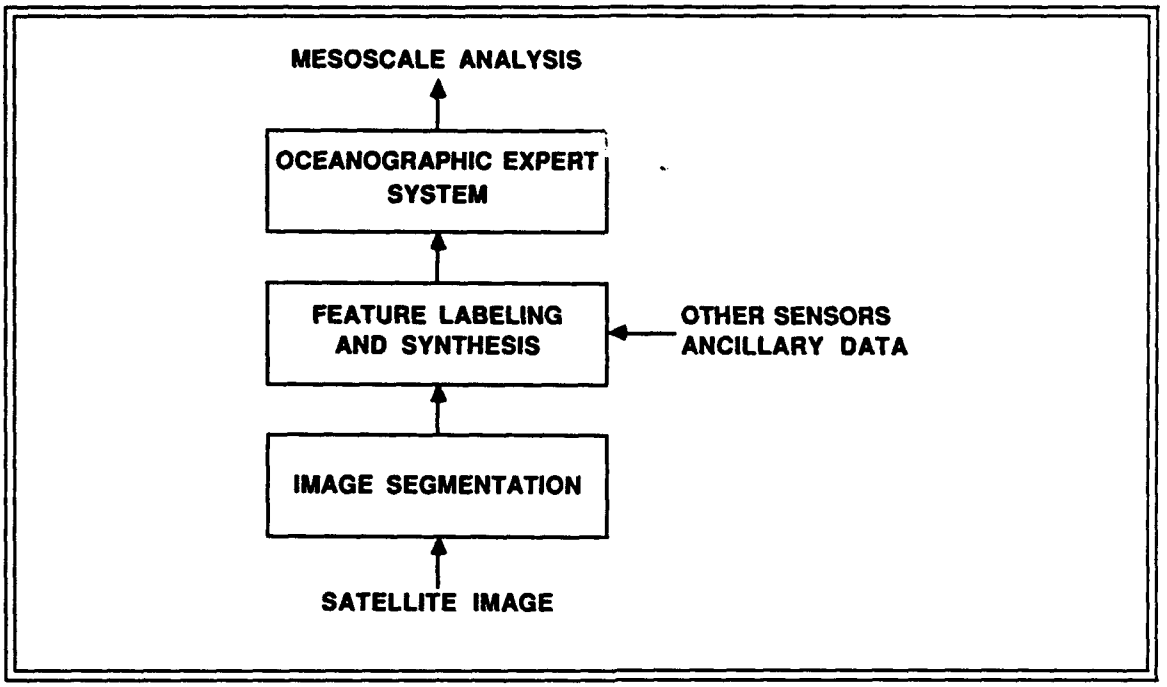

Figure 4. A three-tiered approach to automated oceanographic satellite image analysis. (Adapted from Holyer and Peckinpaugh, 1990)

7.1 Navy's Semi-Automated Mesoscale Analysis System (SAMAS)

A three-tiered approach of SAMAS is shown in Fig. 4, and a functional block diagram is shown in Fig. 5. Although the individual components have been described above, a brief description of the entire system is given here for the sake of completion.

Image Segmentation: Starting with a satellite image, the digitized gray levels are converted into a gray level co-occurence matrix (GLC). The GLC is then used to compute the cluster shade measure, $S(\Delta x = 0, \Delta y = 0)$, in overlapping local neighborhoods. The center point of the neighborhood is then replaced by $S(\Delta x = 0, \Delta y = 0)$. Because this measure is the third central moment of the GLC, it changes sign whenever there is a significant change in the distribution of S over the neighborhood. The specification of the zero-crossings then specifies a frontal pixel.

Feature Labeling and Synthesis: Each frontal-pixel determined in the last step is assigned a feature lable using the Nonlinear Probabilistic Relaxation algorithm. The algorithm assigns different feature probabilities to each pixel, which are improved by successive iteration taking into consideration previous analyses and any new information. The pixels under each feature are then spatially interpolated to construct a continuous GS front or a circular eddy from fragmented renditions of these features. The GS front is interpolated using the complex empirical orthogonal function (CEOF) approach. The CEOF's represent the statistical information extracted from empirical data on the GS front. For each individual image, the modal amplitudes are computed. A weighted sum of these CEOF vectors, with the modal amplitudes as the weights, provides an estimate of the GS front at the present epoch.

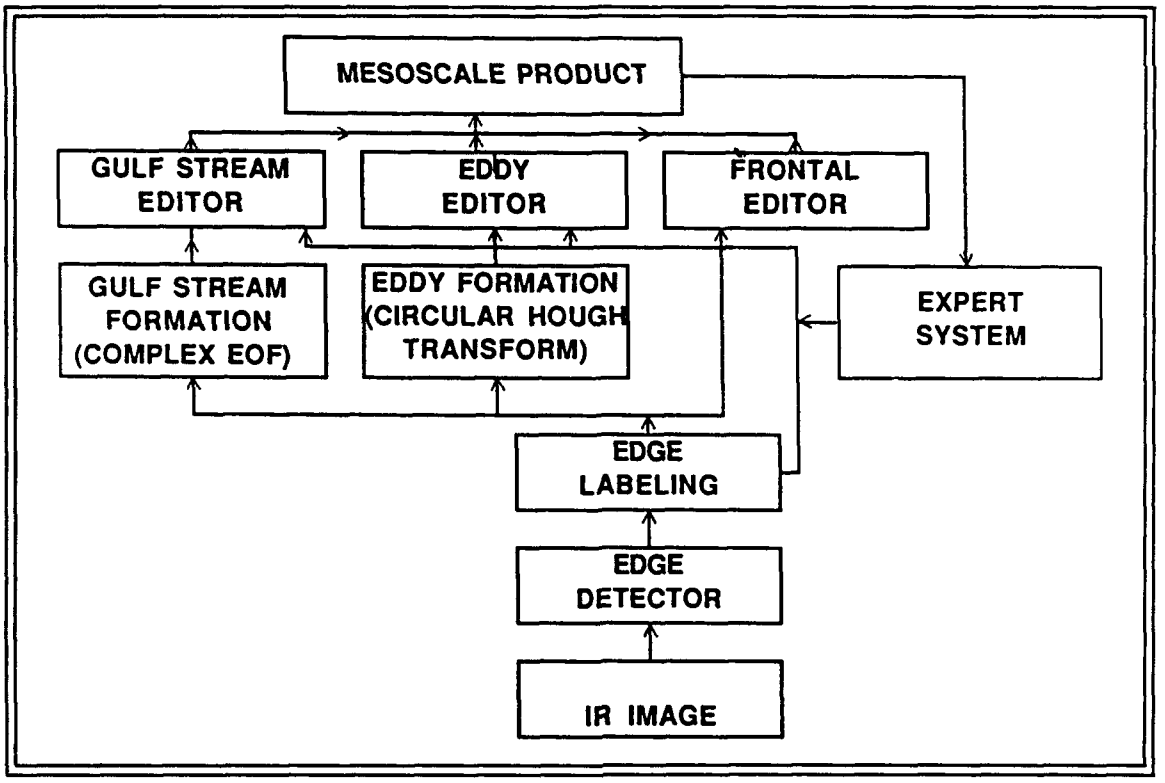

Figure 5. Functional block diagram.

Although not emphasized in Section 6, SAMAS incorporates an eddy synthesis module also, which uses the circular Hough transform (Duda and Hart, 1972). This method is capable of finding the most prominent eddies and gives the center (x_c, y_c) and the radius r even when significant parts of the edge points are missing.

Oceanographic Expert System: The expert system in SAMAS fills in temporal gaps of the features by tracking their evolution in terms of the speed, direction and size (in case of an eddy). It serves an additional function in that it provides a first guess of the feature positions for the Relaxation Labeling Algorithm.

Interactive Editors: The Navy system provides an interactive editing capability for the analyst to view the results and delete and modify the features that are automatically synthesized.

7.2 URI's Feature Detection System

At present, the URI feature detection system does not have all the required components. However, incorporation of a few well-tested modules can make this system a good competitor to the Navy's SAMAS. Their edge detection algorithm is fairly well advanced. Because, the presence of clouds in the image can distort the edges, there is a major emphasis on isolation and removal of clouds from the images. URI has performed a considerable amount of analysis of the AVHRR satellites images of the North Atlantic GS region and provided the resulting edges to the academic community for further research. The algorithm relies on a combination of methods and operates at three levels described below: the picture, the window and the local level. The algorithmic steps are shown in Fig. 6.

Picture Level: This analysis is performed at the overall picture level. The main function at this level

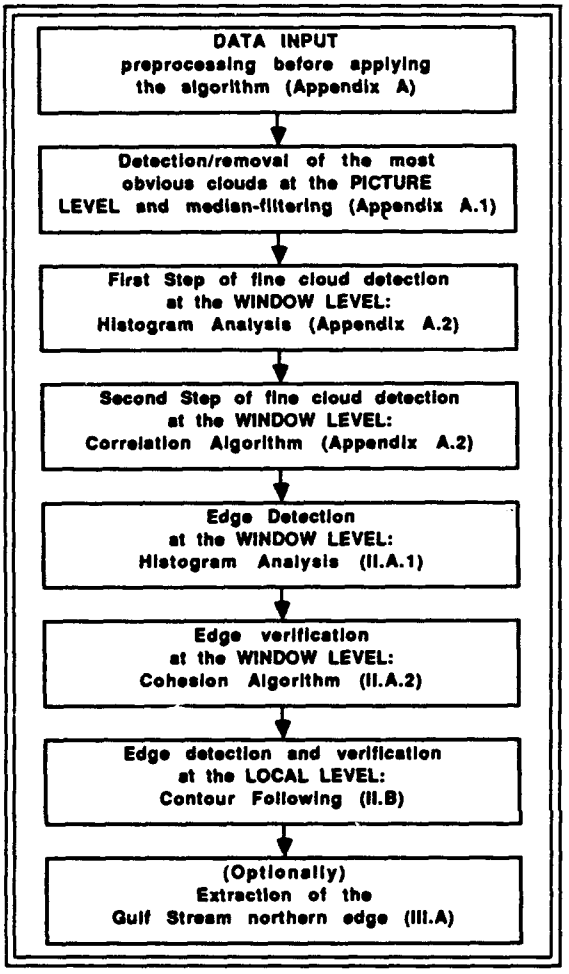

Figure 6. Flowchart of Cayula-Cornillon edge detection algorithm for SST images. (Adapted from Cayula and Cornillon (1992))

is to isolate and remove the obvious cloudy region. The algorithm exploits the physical characteristics to remove the clouds in four steps: (i) Clouds are colder than underlying sea surface, so a rough thresholding is used to separate into non-cloudy and possibly cloudy regions; (ii) Cloudy regions are characterized by high gradient magnitudes that are non-coherent. Thus, if the ratio of the magnitude of the gradient sum to sum of the gradient magnitudes is small/large, classify the region cloudy/clear; (iii) For the regions with an in-between ratio, use the fact that clouds are bulky regions; (iv) finally, use a 3×3 median filter and remove the cloudy regions

Window Level: At this level, the median-filtered data from the Picture Level are examined closely in 32×32 overlapping windows. Each window is processed independently for the presence of an edge. Even at this level, minute attention is paid to removal of clouds that are fine at this stage. A histogram analysis of the temperature values within the window is performed. In the presence of an edge within the window, the histogram will be bimodal, indicating two different temperature populations within the window. The bimodality is statistically tested. This is followed by a correlation analysis to check whether either of the populations could be classified as cloudy. If not, then a cohesion test ensures that the bimodality is actually due to a front and not due to a freak temperature distribution. An indicator function then assigns values of 0 and 1 according to which population the pixel belongs. The boundary of 0s and 1s then defines the edge pixels.

Local Level: At this level, the Contour-Following Algorithm is employed to collect different edge pixels into coherent contours that would represent various fronts and eddies in the mesoscale picture. Analysis beyond this step requires human intervention, as these contours have not been assigned any labels.

8. OTHER OFI EFFORTS

There have been efforts in the atmospheric sciences to objectively analyze satellite data for cloud coverage and radar data to determine gust fronts. For cloud coverage resolution we refer to the recent work of Woodberry, Tanaka, Hendon and Salby (1991). Their work was also motivated from the enormity of the satellite data. Synoptic images of the global cloud cover pattern, composited from six contemporaneous satellites, provide an unprecedented view of the global cloud field. Having horizontal resolution of about 0.5 deg and temporal resolution of 3 hours, the global cloud imagery (GCI) resolves most of the variability of organized convection, including several harmonics of the diurnal cycle. Although the GCI has attractive features, the dense three-dimensional nature of the data make it a formidable

volume of information to treat in a practical and efficient manner. They developed an interactive image analysis system to investigate the space-time variability of the global cloud cover behavior. Their system integrates data, hardware and software into a single system to provide a variety of space-time covariance analyses in a menu-driven format.

Analysts of radar data have been interested in extracting all possible information from radar scans that, like satellites, also provide large amounts of data. Interactive graphical displays of these data have formed the basis for gleaning new knowledge from the radar systems. However, for more practical applications to aircraft safety, there have been efforts to devise an automatic, objective identification of gust fronts using real time radar data. Uyeda and Zrnic (1986) Automatic Detection of Gust Fronts is one such study. They used a pattern recognition algorithm based on radial convergence of winds to determine radial bands of gust-front activity and parameterize them in range and azimuth by fitting the azimuth as a quadratic function of the range.

Similarly, Goodrich et al. (1991) have developed a thin-line detection algorithm to detect associated convergence lines in the radar reflectivity data. For objective feature identification, they also construct a local least squares quadratic model of the reflectivity in terms of range and azimuth.

9. FRONT LOCATION FROM MODEL OUTPUT

Oceanic features like ocean eddies and fronts are three-dimensional features. Unfortunately, observational data in three dimensions are not routinely available in real time to even contemplate their extraction. However, model output is available over time in three dimensions, and it is of considerable importance to extract objectively 3-D features or track their movement over space and time.

There have been efforts to derive features from the model output. One recent study by Fine and Fraser (1990) developed a statistical pattern recognition technique called IREW based on Baye's rule to multiplicatively combine the influence of predictors. Here we focus on two methods that have been recently implemented in CAST for oceanographic visualization. One uses a 3-D edge operator algorithm for feature extraction, while the other uses physical features to track eddies as they move across the region of interest.

9.1 Feature Identification With 3-D Edge Operator

A 3-D edge operator was first used by Zucker and Hummel (1981) for feature detection of CT images defined on unit-spaced pixels. Moorhead and Zhu (1993) extended this operator to work on 3-D data volumes defined on Cartesian grids and irregular grid intervals in one direction and applied it to the numerical output of a Gulf of Mexico model (Dietrich et al., 1993).

Let $f(t, x, y, z)$ be a four-dimensional scalar field defined at time t on the grid point (x, y, z). The algorithm starts by retaining all points (x, y, z) such that

$$\frac{\sigma^2(f(t, x, y, z))}{[E(f(t, x, y, z))]^2} \geq L_t \qquad (29)$$

where L_t is a temporal threshold. This step eliminates time-invariant edges such as the coastlines and noisy data and reduces computational requirements.

For the remaining points, the 3-D edge operator algorithm computes the three Cartesian gradients and then takes the amplitude of their vector sum. The grid points with the maximum composite gradient amplitude defines a neighborhood with the greatest dynamic changes to be tested for oceanic front/eddy detection. This edge computation produces a companion edge volume to the original data volume containing clusters of connected edges. These edge clusters approximate the boundaries of possible features. True features are identified based on the edges. Obviously, it is much more complex to comprehend 3D objects than 2D ones. However,

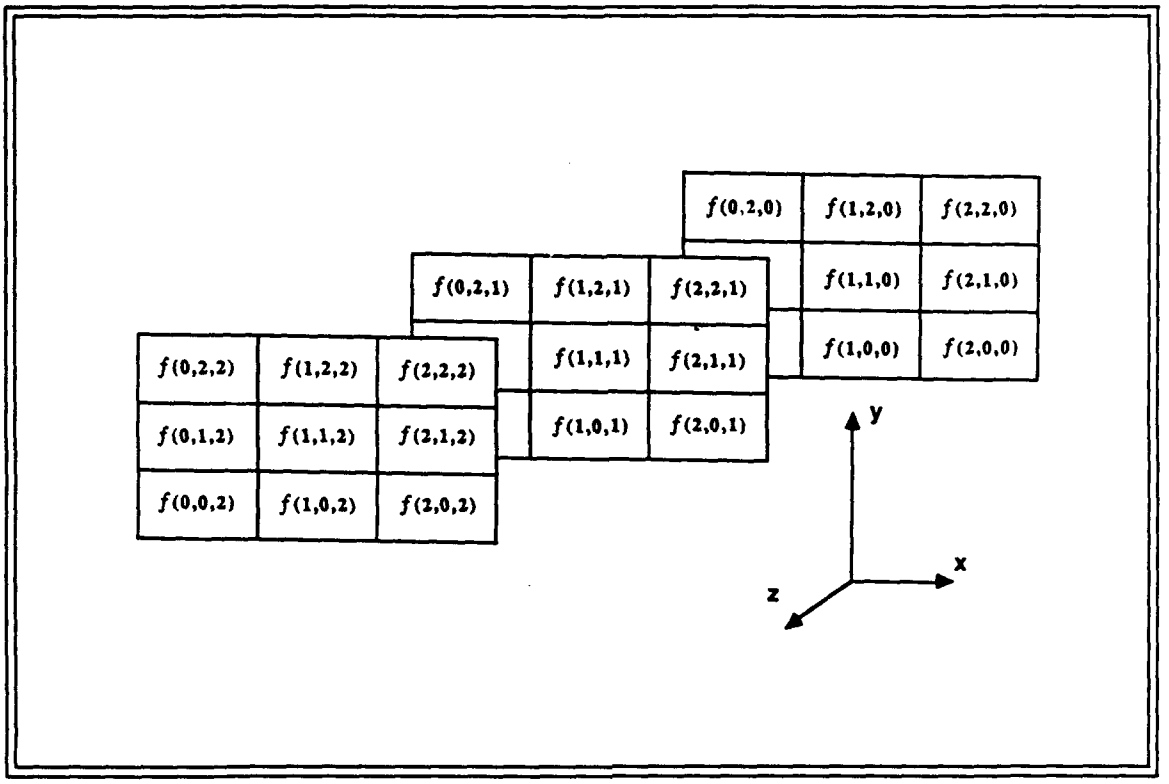

Figure 7. Positional notation for 3 x 3 block.(Adapted from Moorhead and Zhu (1993))

in analyzing oceanographic data sets, strong spatial correlations are found between horizontal data slices within a data volume. Therefore, recognition and reconstruction of 3D features was simplified and speeded up by spatially correlating those features extracted from 2D data slices. Specifically for a feature like eddy, these correlations included functional values, edge values and shapes.

The 3-D edge operator acts on a $3 \times 3 \times 3$ data block around the point under examination. Using the notation of Moorhead and Zhu (1993), at any time t the data in a three-dimensional coordinate system is represented by $f(x, y, z)$; the model output on the gridpoint, (i, j, k) is represented as $f(x_i, y_j, z_k) = f(i, j, k)$. With this notation, a grid point, say $(1, 1, 1)$, is tested for a point on the frontal edge as follows. First, define the $3 \times 3 \times 3$ data block for gradient computation (Fig. 7). For $i, j, k \in \{0, 1, 2\}$, let $\mathbf{V}(i, j, k)$ represent the vector from the origin to the gridpoint (i, j, k), $\mathbf{S}(i, j, k) = \mathbf{V}(i, j, k) - \mathbf{V}(1, 1, 1)$ be the vector difference, $D(i, j, k) = |\mathbf{S}(i, j, k)|$ the distance between the two grid points, and

$$\nabla f(i, j, k) = (f(i, j, k) - f(1, 1, 1))/D(i, j, k).$$

Then the three gradients are defined as:

$$\begin{aligned} \mathbf{g}_x &= \sum_{i,j,k} \nabla f(i, j, k)[\mathbf{S}(i, j, k) \cdot \mathbf{x}]\mathbf{x}, \\ \mathbf{g}_y &= \sum_{i,j,k} \nabla f(i, j, k)[\mathbf{S}(i, j, k) \cdot \mathbf{y}]\mathbf{y}, \\ \mathbf{g}_z &= \sum_{i,j,k} \nabla f(i, j, k)[\mathbf{S}(i, j, k) \cdot \mathbf{z}]\mathbf{z}, \end{aligned} \tag{30}$$

where $\mathbf{x}, \mathbf{y}, \mathbf{z}$ are unit vectors along the respective axes. The amplitude square of the overall gradient is defined as $(|\mathbf{g}_x|^2 + |\mathbf{g}_y|^2 + |\mathbf{g}_z|^2)$.

For application to ocean model output, Moorhead and Zhu assumed constant grid intervals, a and b, along the X and Y directions, and allowed

for a variable interval along the Z direction as z. We note that most of the computational resource in edge detection using the above gradient algorithm is used in computing dot products, which requires evaluation of the three direction cosines, $a(c^2+z^2)^{-1/2}$, $b(c^2+z^2)^{-1/2}$ and $z(c^2+z^2)^{-1/2}$, where $c^2 = a^2 + b^2$ is a constant. To minimize this requirement, they (1) used the approximation, $(c^2+z^2)^{1/2} \simeq c + z^2/2c$, obtained from the second-order Taylor series expansion, and (2) performed these computations in horizontal slices where the Z interval is held constant, so that these square roots are computed once for all. These two steps make the algorithm extremely fast.

At this time, we note the following points:

(i) $\nabla f(i,j,k)$ represents the gradient along the vector $\mathbf{S}(i,j,k)$; the effect of multiplying it with the dot product term in the summations, results in $(f(i,j,k) - f(1,1,1))\cos\theta_s$, where θ_s is the angle that the vector $\mathbf{S}(i,j,k)$ makes with the s-axis, $s \in [X,Y,Z]$. Thus, the terms in summation are the total change being resolved along the different axes.

(ii) If a point were to lie in a volume of f values that are at most varying linearly in x, y and z, then $\mathbf{g}_x, \mathbf{g}_y$ and $\mathbf{g}_z$ will be almost negligible. This is easy to see since the point $(1,1,1)$ lies in the symmetric center of the $3 \times 3 \times 3$ cube, and for each $\nabla f(i,j,k)$ there is a symmetric difference of equal magnitude but opposite sign. If the point being tested were to lie inside the eddy, then for small grid lengths we could assume a linear variation. On the other hand if the point were outside the eddy, it would be in volume of almost constant f values.

(iii) For a point on the boundary of an eddy, it is in the middle of two neighborhoods, one of eddy characteristics and the other with non-eddy characteristics. The functional difference from the eddy side will contribute something that is stronger than a linear variation (perhaps involving a jump), while the non-eddy side will contribute ~ 0. Thus, the above formulation is quite appropriate to make the edge (or boundary points) stand out from the rest.

(iv) It may be possible to come up with a statistical test to the null hypothesis of a grid point, along with its neighboring points in the $3 \times 3 \times 3$ cube, completely lying within a linearly-varying volume. Under this null hypothesis, we can form thirteen double sums of $\nabla f(i,j,k)$ e,g., $(\nabla f(2,2,2) + \nabla f(0,0,0))$, each having zero mean and the same variance. The number thirteen results from the twenty-six $\nabla f(i,j,k)$, nine each from $k = 0, 2$ and eight from $k = 1$ (See Fig. 7). Denoting these double sums by s, their mean by $\bar{s}$, and assuming them to be statistically independent (which they are not, since each sum contains $2f(1,1,1)$ as common), the statistic

$$t = \frac{\bar{s}}{\sum s^2} \tag{31}$$

is distributed approximately as Student's t with 13 degrees of freedom.

Even without this test of hypothesis, the algorithm is quite efficient in extracting ocean eddies from model outputs. The algorithm developed is general and may be applied to various ocean features by specifying different identification criteria. The performance of this algorithm was demonstrated on the DieCAST model output for the Gulf of Mexico region. An example of the sharpness of the eddy features extracted using the algorithm is shown in Fig. 8.

9.2 Objective Tracking of an Eddy

In order to analyze the thermodynamic structure of the ocean circulation simulated by a numerical ocean model, it is necessary to sequentially observe, in time and space, mesoscale features manifested by the model output. Because of grid dimensions, as well as the frequency of sampling, such examinations are ponderous at best. The algorithm developed here objectively tracks an eddy over time

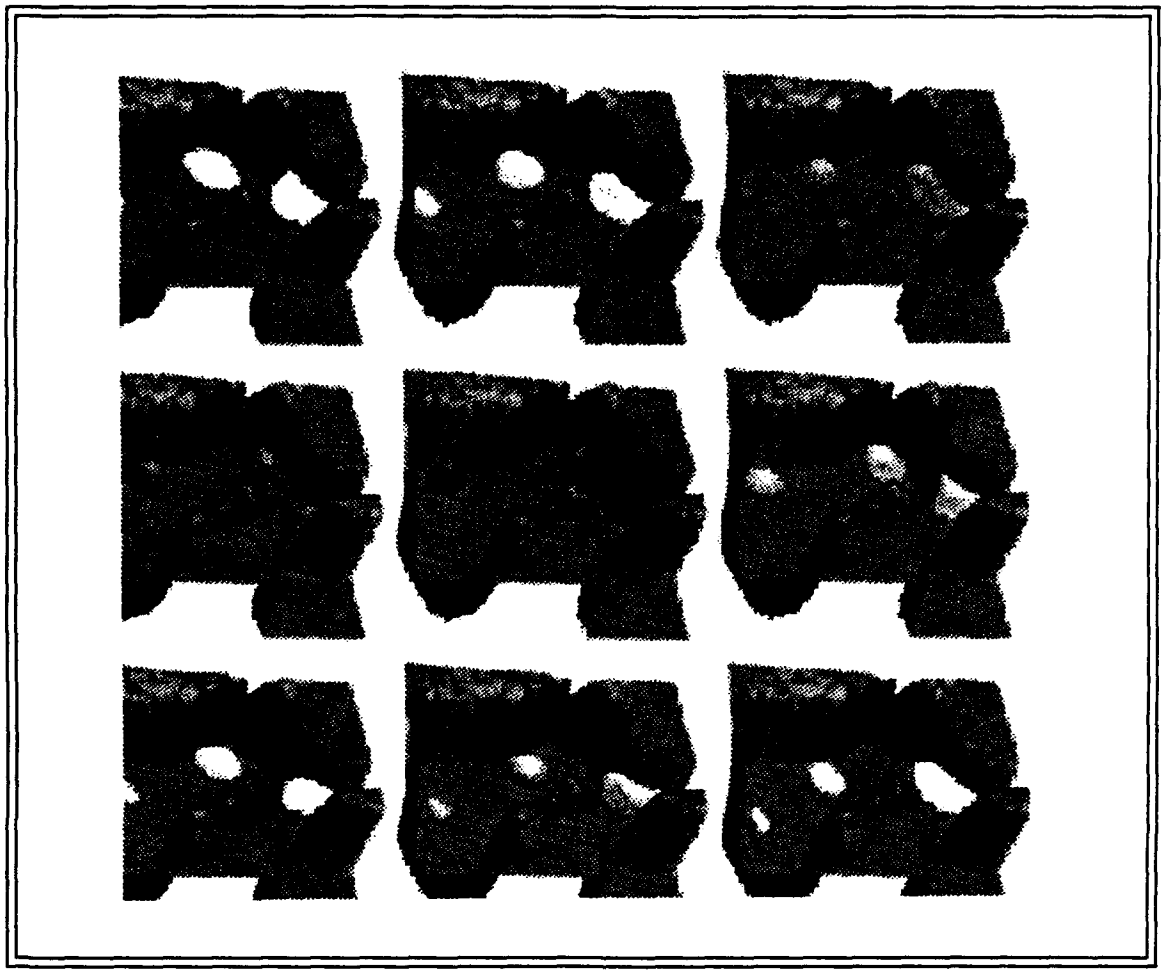

Figure 8. An example of extracted eddies that are animated temporally to show their characteristics variations. The sequence progresses from left to right and top to bottom (lexographical order). (Adapted from Zhu et. al. (1993))

and space. To initiate the tracking process, model output is displayed on the screen so that the region of activity, the to-be-tracked eddy, is identified. From this point on, the algorithm homes in on the eddy as it evolves over time and space.

The eddy can be tracked with respect to any of the thermodynamic parameters, e.g., SSH, SST, speed of eddy circulation, etc. For further sophistication, one may utilize the subsurface values. However, the purpose of this algorithm is to follow the general movement of the eddy; that includes a general neighborhood of the eddy activity without specifying an exact eddy center.

Objective Tracking Criterion: The derivation of this algorithm depends on the monotonic behavior of the various parameters employed in the tracking. For instance, if the eddy is a cyclonic eddy and SST is used to track its motion, then the eddy is a warm core eddy, characterized by monotonically-decreasing temperatures as we move away from the eddy center. If the temperature of the eddy surface is viewed in three dimensions, it will look like an inverted paraboloid (See Fig. 9a). Similarly, if SSH is used for tracking, the sea surface elevation will be maximum at the eddy center, and it will

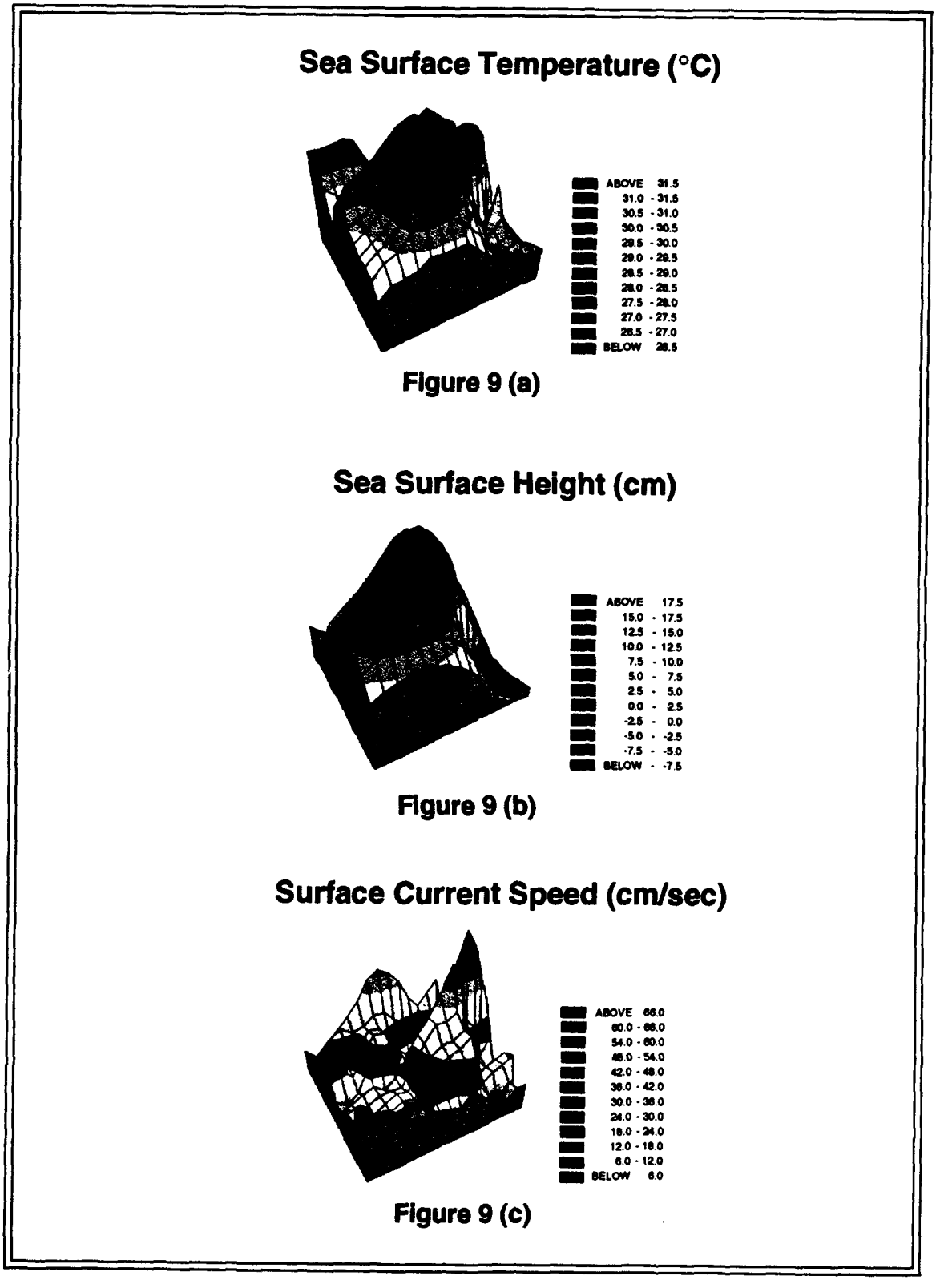

Figure 9. A three dimensional presentation of a warm-core eddy in terms of its (a) sea-surface temperature, (b) sea-surface height and (c) surface current speed. Note that the minimum current speed occurs at the center of the eddy.

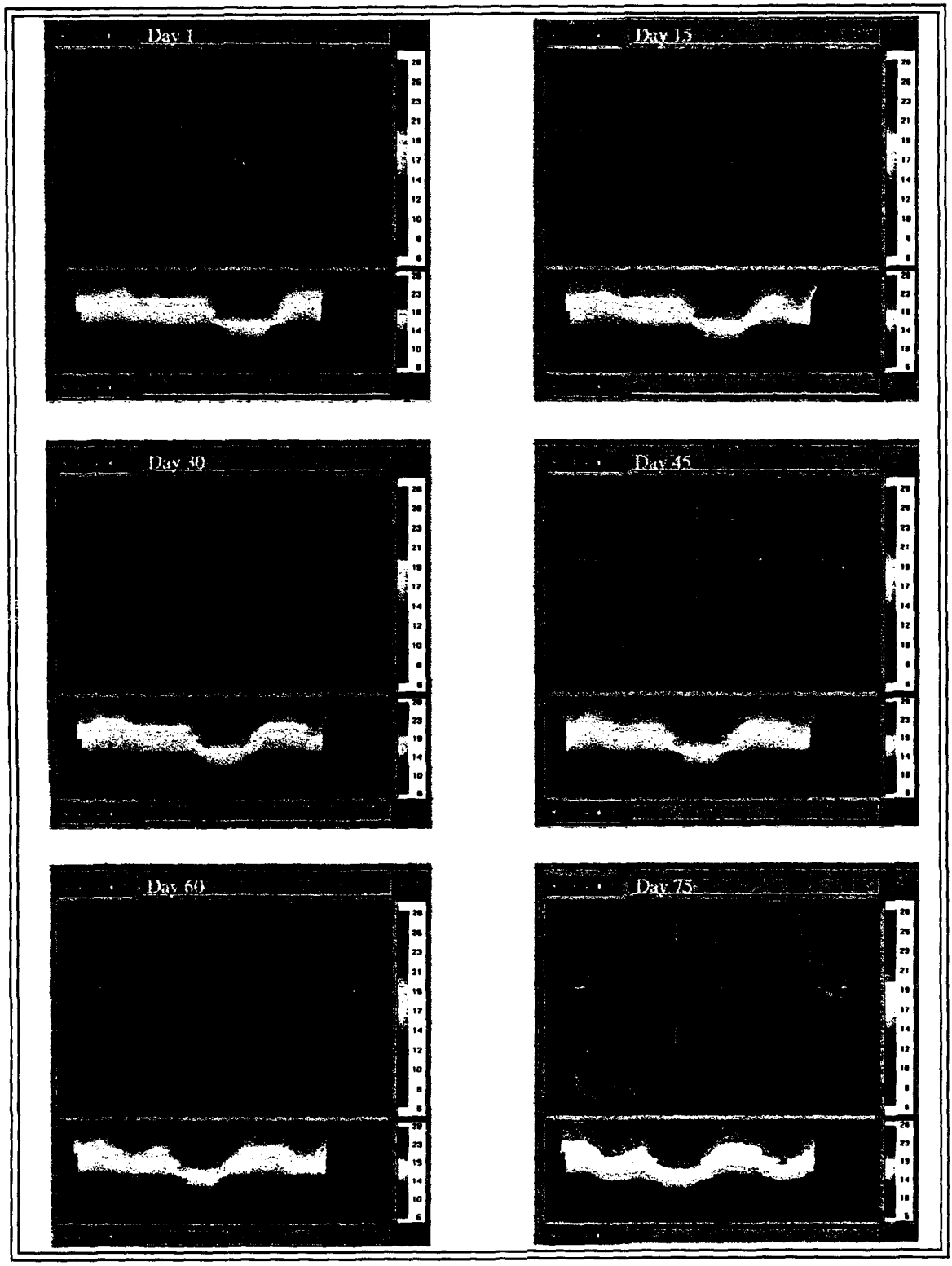

Figure 10. Six images of an animated sequence of two synchronized windows for eddy tracking. Window 1 (upper) is the horizontal cross-section of the temperature field with the cross-hair at the eddy center and window 2 (lower) is the vertical (XZ) cross-section at the latitude of the eddy center represented by the cross-hair. (Adapted from Lakhamaraju (1993))

circulation in terms of SSH. However, if current speed is the criterion, then the speed at the eddy center is the minimum, and it increases as we move away from the center. In fact, it has been observed in the Gulf of Mexico that eddies rotate as a solid body. A three-dimensional graph of speed of eddy currents will appear like a parabola, with its vertex at the minimum (Fig. 9c). Thus for a selected parameter, the algorithm invokes its monotonic behavior, fits the parameter to a local, two-dimensional smooth surface as a function of X-longitude and Y-latitude, and finds a local extreme point. Because of the monotonic behavior of the eddy circulation parameters, this extreme point will be a maximum for SST and SSH and a minimum for the current speed. In any case, this extreme point will determine the eddy center. Fig. 10 displays six images of on animated sequence of two synchronized windows for eddy tracking.

Least Squares Formulation: Let (x, y) be the location in terms of (longitude, latitude). Then, given an approximate starting position of the eddy center, (x_0, y_0), select all grid points within a radius R. Let us fit

$$\zeta = ax^2 + bxy + cy^2 + dx + ey + f \qquad (32)$$

where ζ is the value of parameter used to characterize the eddy (SSH, SST, or current speed) at locations (x, y). Once the quadratic surface in eq. (32) is specified, we can find its extreme point by equating to zero the first derivatives with respect to x and y, i.e.,

$$\begin{aligned} 2ax + by + d &= 0 \\ bx + 2cy + e &= 0 \end{aligned} \qquad (33)$$

Solving eq. (33), we estimate the eddy center by

$$\begin{aligned} x_1 &= \frac{be - 2cd}{4ac - b^2}, \\ y_1 &= \frac{bd - 2ae}{4ac - b^2}. \end{aligned} \qquad (34)$$

Assuming that the time interval between eddy tracking is moderate, one can derive the next guess using the newly-estimated eddy center position (x_1, y_1) and modifying by incorporating the past information on the eddy center velocity and then repeating the steps described above.

In fitting the quadratic least squares surface eq. (32), it will be necessary to rearrange the indices so that one can cast eq. (32) in a standard format:

$$\mathbf{Y} = \mathbf{X}\boldsymbol{\beta}$$

where $\mathbf{Y}$ is the vector obtained from rearranging ζ_{ij} in a single vector; $\boldsymbol{\beta} = (\beta_1, \ldots \beta_6)^t$, with $\beta_1 = a$, $\beta_2 = b$, $\beta_3 = c$, $\beta_4 = d$, $\beta_5 = e$ and $\beta_6 = f$; $\mathbf{X} = (X_{k,l})$ is $n \times 6$ matrix with the index k corresponding to the observation index of Y_k and j corresponding to the parameter index of β_l. Suppose the index k corresponds to the grid point (i, j), then $X_{k1} = x_{ij}^2$, $X_{k2} = x_{ij}y_{ij}$, $X_{k3} = y_{ij}^2$, $X_{k4} = x_{ij}$, $X_{k5} = y_{ij}$ and $X_{k6} = 1$.

The following simple steps are involved. Start with initial position $p_I = (x_I, y_I)$ and assume the initial eddy center velocity $V_1 = (V_x, V_y)$ is zero. Say we have determined eddy centers $p_j = (x_j, y_j)$ at times $t_j, j = 1, \cdots, n$. The initial position for the next step is defined by $p_I = p_n + V_n(t_{n+1} - t_n)$ at time t_n, where $V_n = \frac{p_n - p_{n-1}}{t_n - t_{n-1}}$, with $V_1 = 0$ All grid points within the specified radius R of (x_I, y_I) are then determined and the two-dimensional array ζ_j and (x_{ij}, y_{ij}) are loaded into Y_k and X_{kl}. A least squares algorithm is used to determine coefficients $\boldsymbol{\beta}$ that are interpreted in terms of eq. (32). Solve eq. (33) to find $p_{n+1} = (x_{n+1}, y_{n+1})$.

10. CONCLUDING REMARKS

We have provided a brief review of objective methods that have been used for identification and tracking of mesoscale ocean features like eddies and fronts. The North Atlantic, Gulf Stream region has been the main area of feature identification, primarily because of the well-defined, sharp features of the Gulf Stream, the large amounts of data available from a large number of experiments conducted, and because of Navy interest in the region. Also, the region enjoys availability of large amounts of remotely sensed, satellite data providing information on SST and SSH. Thus, most of the methodologies developed and reviewed pertain to the GS region.

used by the oceanography community in its analyses of the various kinds of data. In our view, the best objective method would be to dynamically interpolate the available information by appropriate data assimilation methods and extract the features of interest. This approach will take advantage of all possible data, surface or sub-surface, and will dynamically interpolate the features in the missing part of the satellite image. The features can be extracted by interpolating for the specific feature characteristics, e.g., the T_{15}, the 15 deg isotherm at 200 m depth to determine the GSNW or use the general edge detection procedures of Section 5. This takes both data and dynamics into consideration. This capability is still somewhere in the future, since the ocean models have not attained the necessary maturity.

As an alternative, the four-tiered algorithmic approach fostered by Lybanon and Holyer (1991) comprising edge detection, edge labeling, feature construction and the expert system is quite appropriate. The modular approach adopted in the Navy's SAMAS promises to be an excellent system. Improvements and modifications to individual modules can be affected independently.

The edge detection system based on the Cluster Shade Edge Operator functions well and seems to avoid the noisiness of the gradient-type edge operators. It is based on the (fun-normalized) skewness measure of the gray-level co-occurrence matrix. In evaluation of five different edge detection algorithms, Cornillon and Watts (1987) also found the 'skew' algorithm to be the best. Most analyses performed on the GS front detection are based on the initial analyses of the satellite images performed by the URI group. The edge detection and contour following algorithm of Cayula and Cornillon (1992) is quite sophisticated and is based on objective, statistical methodology that effectively and systematically eliminates the effect of clouds in satellite images. However, the URI system still needs to develop the subsequent components of the four-tiered approach mentioned above.

The feature labeling algorithm of Krishnakumar et al. (1990a) is an imperative step in the development of an automatic feature identification system. This algorithm is based on the Bayes probability, and it iteratively updates the probability of assigning a pixel its feature label.

For spatial interpolation, and for temporal interpolation to some extent, the best approach would be to use a Kalman-type model. This approach can easily incorporate two-dimensional phase speeds of complex meanders and take advantage of estimations in the past to arrive at an optimal estimation at the current epoch. This approach has the additional advantage of providing estimation error in terms of the estimated covariance parameters. But even for this best approach, Chin and Mariano (1993) indicate that it cannot yet realize the sensitivity of the trained personnel. Perhaps, the only advantages over the manual approach are the objectivity, consistency and savings in time.

The methods based on the data and statistical correlations would be next in order. The Pathfinder model, to determine the mean GS axis using an objective interpolation approach, correlates the across-stream anomalies using a parametric covariance structure that is a function of the along-stream distance. We were surprised that this method did not work as well as one might expect. But as Horton (1982) conjectures, the problem may be confounded by mis-specification of the mean GS axis and of the covariance structure, and also the large variance around the axis. For an evaluation of the Pathfinder and some other algorithms, see Szczechowski (1992).

The method based on complex empirical orthogonal function is also based on the correlations of the GS positions along the axis, but it avoids parameterization of the covariance function. However, the method requires updating of the complex amplitudes based on few, new positional fixes. This was done using nonlinear least squares optimization.

In a different analysis based on inverted echo sounders and other estimation procedures, Cornillon and Watts (1987) found that the objective methods were, at most, as accurate as the subjective analysis of the GSNW as defined by T_{15}. The rms error

varied from 15 to 30 km. Passi et al. (1991) using an analysis of tomographic data, which is quite accurate, indicated that the limit of prediction of the GSNW was about 7 km. Such estimation accuracy appears to be far in the future.

The GSNW meanders are quite complex in shape and often occur in shapes like 'S' and 'Ω'. It is quite obvious that simple spline-type interpolation schemes, where the longitude is a function of the latitude as the independent variable, could not resolve such multivalued meanders. From a close examination of the statistical approaches reviewed, we notice that all of them employ the arc length of the GS as the coordinate of reference, which is quite an ingenious approach.

Horton (1982) used the GS climatology as the coordinate of reference and utilized observations within a fixed time frame, assigning weights according to the age of the observation, to perform optimum interpolation. However, the algorithm does not incorporate information from the past estimations.

Molinelli and Flanigan (1987) used individual axes for their CEOF estimation. The latitude of their starting reference point varied but had 75°W as the longitudinal point. They employed the past estimation of the GS axis only as an initial guess in the nonlinear least squares estimation at the current epoch. Thus, the past estimation was incorporated in the sense that it was modified to conform with the new information.

However, it was Mariano (1990) who clearly stated that a dynamic frame of reference in terms of the arc length of the GS was clearly the most logical choice as the coordinate of reference. He employed one-dimensional phase speeds to adjust the past and future information on the GS to interpolate in the present. Chin and Mariano (1993) took this approach to the next logical formulation of the Kalman filtering.

In the final analysis, the four-tiered approach adopted by the Navy in the development of SAMAS is an important step in taking advantage of the ever-increasing amounts of satellite data. It is anticipated that the system will be constantly upgraded as the new algorithms are developed and tested.

ACKNOWLEDGMENTS

The authors are grateful to Mr. James Corbin and Dr. Lanny Yeske for their comments on the paper, and to Ms. Susan Sprouse for her technical editing. We also appreciate the efforts of MSU's Steve Foster, Evelyn Lott and Carolyn Michael in preparing this document. This research was supported by the Office of Naval Research's Navy Ocean Modeling and Prediction Program under Research Grants N00014-92-J-4112 and N00014-92-J-4109 (Passi and Anand).

REFERENCES

Albano, 1974: Representation of digitized contours in terms of conic arcs and straight-line segments. *Comput. Graph. Image Processing*, 3, 23-44.

Bevington, P.R., 1969: *Data reduction and error analysis for the physical sciences*, McGraw-Hill, New York.

Bretherton, F.P., R.E. Davis, and C.B. Fandry, 1976: A technique for objective analysis and design of oceanographic experiments applied to MODE-73. *Deep-Sea Research*, 23, 559-582.

Carter, E.F., 1985: The structure of the Gulf Stream as derived from an EOF analysis. *Gulf Stream Workshop Proceedings*, University of Rhode Island.

Cayula, J.F., and P. Cornillon, 1992: Edge detection algorithm for SST images. *J. Atmosph. Ocean. Tech*, 9, 67-80.

Chin, T.M., and A.J. Mariano, 1993: Optimal space-time interpolation of gappy frontal data. *statistical Methods in Physical Oceanography, Proceedings 'Aha Huliko'a Hawaiian Winter Workshop*, University of Hawaii at Manoa, January, 12-15, 1993.

Conners, R.W., M.M. Trivedi, and C.A. Harlow, 1984: Segmentation of a high-resolution urban

scene using texture information. *Computer Vision, Graphics and Image Processing*, 25, 273-310.

Cornillon, P., and D.R. Watts, 1987: Satellite thermal infrared and inverted echo sounder determinations of the Gulf Stream northern edge. *J. Atmosph. Ocean. Tech*, 4, 712-23.

Cummings, J.A., 1991: Water mass empirical orthogonal functions in the NW Atlantic with applications to optimal field estimation. *Unpublished Report, Fleet Numerical Oceanography Center.*

Dietrich, D.F.,D.-S. Ko and L.A. Yeske, 1993: On the application of the relocatable DieCAST ocean circulation model in coastal and semi-enclosed seas. *Center for Air Sea Technology Technical Report 93-1*, Stennis Space Center, MS., 71 pp.

Duda, R.O., and P.E. Hart, 1972: Use of the Hough transform to detect lines and curves in pictures. *Commun. ACM*, 15, 11-15.

Duda, R.O., and P.E. Hart, 1973: *Pattern Recognition and Scene Analysis.* John Wiley and Sons, 482 pp.

Fine, S.S., and A.B., Fraser 1990: A Simple Technique for Multiple-Parameter Pattern Recognition with an Example of Locating Fronts in Model Output. *Journal of Atmospheric and Oceanic Technology*, 7, 896-908.

Fox, D.N., M.R. Carnes and J.L. Mitchell, 1991: Gulf Stream mesoscale forecasting. *MTS '91 Proc.*, Marine Technology Society, 411-17.

Gelb, A., Editor, 1974: *Applied Optimal Estimation.* MIT Press, Cambridge, MA.

Goodrich, R.K., F.W. Wilson, Jr. and D. Rogers, 1991: A thin line detection algorithm. *25th International Conf. on Radar Meteor.*, Paris.

Holyer, R.J., and S.H. Peckinpaugh, 1989: Edge detection applied to satellite imagery of the oceans. *IEEE Trans. Geo. Rem. Sens.*, 27, 46-56.

Holyer, R.J., and S.H. Peckinpaugh, 1990: Evaluation of the Navy's Semi-Automated Mesoscale Analysis System (SAMAS). *Proc. Fifth Conf. on Satellite Meteor., London Eng., Amer. Meteor. Soc.*, 202-207.

Horton, C.W., 1982: Preliminary report on inferring the path of the subsurface front of the Gulf Stream from infrared observations. *US Naval Oceanographic Office TN 9100-9-81*, US Naval Oceanographic Office, NSTL, MS.

Horton, C.W., 1989: An overview of the reliability of the Gulf Stream Pathfinder Algorithm. Naval Oceanographic Office internal memo.

Kittler, J. and J. Illingworth 1985: Relaxation labeling algorithms - a review. *Image and Vision Computing* 3(4),, 206-216.

Krishnakumar, N., and S.S Iyengar, R. Holyer and M. Lybanon 1990a: Feature labeling in infrared oceanographic images. *Image and vision computing*, 142-147.

Krishnakumar, N., and S.S Iyengar, R. Holyer and M. Lybanon 1990b: An expert system for interpreting mesoscale features in oceanographic satellite images. *Int. J. Pattern Recog. and Art. Intelligence*, 4, 341-355.

Krishnakumar, N., and S. S Iyengar, 1991: A hybrid technique for interpreting mesoscale analysis system (SAMAS). *Proceedings: Automated interpretation of oceanographic satellite images workshop.* Naval Oceanographic and Atmospheric Research Laboratory, Stennis Space Center, MS NOARL Report SP 001:321:91, 37-48.

Lakhamanraju, L.R. 1993: Two-Dimensional CAST Ocean Visualization system *Center for Air Sea Technology Technical Note 02-94*, Stennis Space Center, MS., 13-15.

Landau, U.M., 1987: Estimation of a circular arc center and its radius. *Comput. Vis. Graph. Image Processing*, 38, 317-326.

Lewis, F.L., 1986: *Optimal Estimation.* John Wiley & Sons, New York.

Lybanon, M., Ed., 1991: *Proceedings: Automated interpretation of oceanographic satellite images workshop.* Naval Oceanographic and Atmospheric Research Laboratory, Stennis Space Center, MS NOARL Report SP 001:321:91, 226 pp.

Lybanon, M. and R.J. Holyer, 1991: Historical overview of NOARL automated imagery interpretation studies. *Proceedings: Automated interpretation of oceanographic satellite images workshop.* Naval Oceanographic and Atmospheric Research Laboratory, Stennis Space Center, MS NOARL Report SP 001:321:91, 3-8.

Mariano, A.J., 1988: Space-time interpolation of Gulf Stream north wall positions. Harvard Open Model Reports, (29), *Reports in Meteorology and Oceanography*, Harvard University.

Mariano, A.J., 1990: Contour analysis: A new approach for melding geophysical fields. *J. Atmosph. Ocean. Tech*, 7, 285-295.

Molinelli, E.J., and M.J. Flanigan, 1987: Optimized CEOF interpolation of the Gulf Stream. *Planning Systems Incorporated Technical Report No. TR-992995*, prepared for Naval Ocean Research Development Activity, Code 321, NSTL Station, Mississippi 39529,

Moorhead, R.J., Z. Zhu, 1993: Feature extraction for Oceanographic Data Using a 3D Edge Operator. *IEEE Visualization '93 Proc.*, 402-405.

Passi, R.M., H. Anand and S. Foster, 1991: Statistical evaluation of acoustic travel time in locating ocean fronts. *MTS '91 Proc.*, Marine Technology Society, 294-298.

Peckinpaugh, S.H., 1991: An improved method for computing gray-level co-occurrence matrix based texture measures. *Graphical models and image processing*, 53, 574-580.

Peckinpaugh, S.H., and R.J. Holyer, 1991: Evaluation of the Navy's semi-automated mesoscale analysis system SAMAS). *Proceedings: Automated interpretation of oceanographic satellite images workshop.* Naval Oceanographic and Atmospheric Research Laboratory, Stennis Space Center, MS NOARL Report SP 001:321:91, 57-70

Peckinpaugh, S.H., and R.J. Holyer, 1994: Circle detection for extracting eddy size and position from satellite imagery of the ocean. *IEEE Trans. Geo. Rem. Sens.*, 32, 267-273.

Perkins, L., 1993: DAMEE-GSR Phase 0: OTIS Initialized One-Week Forecasts. *Center for Ocean & Modeling Technical Report 1-93*, 63pp.

Robinson, A.R., and L.J. Walstad 1987: The Harvard Open Ocean Model: Calibration and application to dynamical process, forecasting and data assimilation. *J. Appl. Numer. Math.*, 3(1-2), 89-131.

Robinson, A.R., W.G. Leslie, L.J. Walstad and D.J. McGillicuddy, 1987: Gulfcasting: Dynamical forecast experiments for Gulf Stream meanders - November 1985-June 1986. Harvard Open Ocean Reports, 22, *Reports in Meteorology and Oceanography*, Harvard University.

Szczechowski, C., 1991: The Marr-Hildreth operator as an eddy detector. *Proceedings: Automated interpretation of oceanographic satellite images workshop.* Naval Oceanographic and Atmospheric Research Laboratory, Stennis Space Center, MS NOARL Report SP 001:321:91, 153-168.

Szczechowski, C., 1991: Comparison of satellite-derived Gulf Stream front and eddy analyses with GEOSAT underflight AXBT data. *MTS '91 Proc.*, Marine Technology Society, 227-35.

Thomas, S.M., and Y.T. Chan, 1989: A simple approach for the estimation of a circular arc center and its radius. *Comput. Vis. Graph. Image Processing*, 45, 362-70.

Uyeda, H., and D.S. Zrnic, 1986: Automatic detection of gust fronts. *J. Atmosph. Ocean. Tech*, 3, 36-50.

Woodbury K., K. Tanaka, H. Hendon and M. Salby 1991: An Interactive System for Analysis of

Global Cloud Imagery. *American Meteorological Society*, 627-638.

Zucker, S.W., and R.A. Hummel, 1981: A 3D edge operator, *IEEE Trans. PAMI*, 3, 324-331.

Zhu, Z., L. R. Raju, R.J. Moorhead and H. Anand, 1993: Feature extraction and tracking in Oceanographic Visualization. *To be published in SPIE '94 Proc.*

DISTRIBUTION LIST

Scientific Officer Code 1242
Robert A. Peloquin (3)
Office of Naval Research
800 North Quincy Street
Arlington, VA 22217-5000

Office of Naval Research
800 North Quincy Street
Arlington, VA 22217-5000
Emanuel Fiadeiro
Alan Weinstein

Administrative Grants Officer
Office of Naval Research
Resident Representative N66020
Administrative Contracting Officer
Georgia Institute of Technology
206 O'Keefe Building
Atlanta, GA 30332-0490

Defense Technical Info Center (2)
Building 5, Cameron Station
Alexandria, VA 22304-65145

Naval Research Laboratory
Washington, DC 20375-5000
Code 2627

Naval Research Laboratory
Stennis Space Center, MS 39529
John Harding
Harley Hurlburt
Joe McCaffrey

Naval Research Laboratory
Monterey, CA 93943-5006
Ted Tsui

Naval Meteorology and Oceanography
Command
Building 1020
Stennis Space Center, MS 39529
Don Durham

Fleet Numerical Meteorology and
Oceanography Center
Monterey, CA 93943
Mike Clancy
James Cummings

Naval Oceanographic Office
Stennis Space Center, MS 39529
Landry Bernard
Steve Haeger
Martha Head

William J. Schmitz
Woods Hole Oceanographic Institution
Woods Hole, MA 02543

MSU Office of Research
Mississippi State, MS 39762
Ralph Powe
Melvin Ray

University of Southern Mississippi
Building 1103
Stennis Space Center, MS 39529
Ranjit Passi
Germana Peggion
Louise Perkins
Robert Willems

SPAWARS PMW-175-3B
2451 Crystal Drive
Arlington, VA 22245-5200
David Markham
Edward Harrison

REPORT DOCUMENTATION PAGE

Form Approved
OMB No. 0704-0188

1. Agency Use Only *(Leave blank).*	2. Report Date.	3. Report Type and Dates Covered.
	15 SEPTEMBER 1994	TECHNICAL REPORT

4. Title and Subtitle.
OBJECTIVE FEATURE IDENTIFICATION AND TRACKING: A REVIEW

5. Funding Numbers.
Program Element No.
Project No.
Task No.
Accession No.

6. Author(s).
RANJIT M. PASSI
HARSH ANAND

7. Performing Organization Name(s) and Address(es).
MISSISSIPPI STATE UNIVERSITY
CENTER FOR AIR SEA TECHNOLOGY
STENNIS SPACE CENTER, MS 39529

U. SOUTHERN MISSISSIPPI
CENTER FOR OCEAN/
ATMOSPHERIC MODELING
STENNIS SPACE CENTER, MS
39529

8. Performing Organization Report Number.
CAST TECHNICAL
REPORT 94-4

9. Sponsoring/Monitoring Agency Name(s) and Address(es).
OFFICE OF NAVAL RESEARCH
800 NORTH QUINCY STREET
CODE 1242
ARLINGTON, VA 22217-5000

10. Sponsoring/Monitoring Agency Report Number.
REPORT 94-4

11. Supplementary Notes.
RESEARCH PERFORMED UNDER OFFICE OF NAVAL RESEARCH CONTRACT/GRANTS NO. N00014-92-J-4109 AND N00014-92-J-4112

12a. Distribution/Availability Statement.
APPROVED FOR PUBLIC RELEASE: DISTRIBUTION IS UNLIMITED

12b. Distribution Code.

13. Abstract *(Maximum 200 words).*

Remote sensing of the oceans via satellites is providing data that can be used for realtime input into and verification of numerical ocean models, and efficient methods are being developed to handle the vast amounts and provide for quick analyses. There is also considerable interest in designing algorithms to automatically detect oceanographic features such as fronts and eddies. This report provides a literature review of recent efforts on objective feature identification. The literature reviewed here pertains to the Gulf Stream entirely, but is applicable to other geographical features of interest. Feature identification from satellite data can be viewed as a four-step process: (1) edge detection; (2) edge labeling; (3) spatial interpolation; and (4) expert system. Considerable effort is required to design a system to go from raw satellite imagery to a finished product in terms of digitized frontal location and dynamics. The Navy's Semi-Automated Mesoscale Analysis System (SAMAS) is perhaps the only system that has combined these steps in a modular approach, although another image analysis system has been developed at the University of Rhode Island (URI). Brief descriptions of SAMAS and the URI systems are provided. Finally, methods of feature extraction and eddy tracking from model output are described.

14. Subject Terms.
(U) OBJECTIVE (U) FEATURE (U) IDENTIFICATION (U) OCEAN
(U) MODEL (U) GULF STREAM (U) FRONTS (U) EDDIES (U) SAMAS
(U) URI

15. Number of Pages.
39

16. Price Code.

17. Security Classification of Report.	18. Security Classification of This Page.	19. Security Classification of Abstract.	20. Limitation of Abstract.
UNCLASSIFIED	UNCLASSIFIED	UNCLASSIFIED	